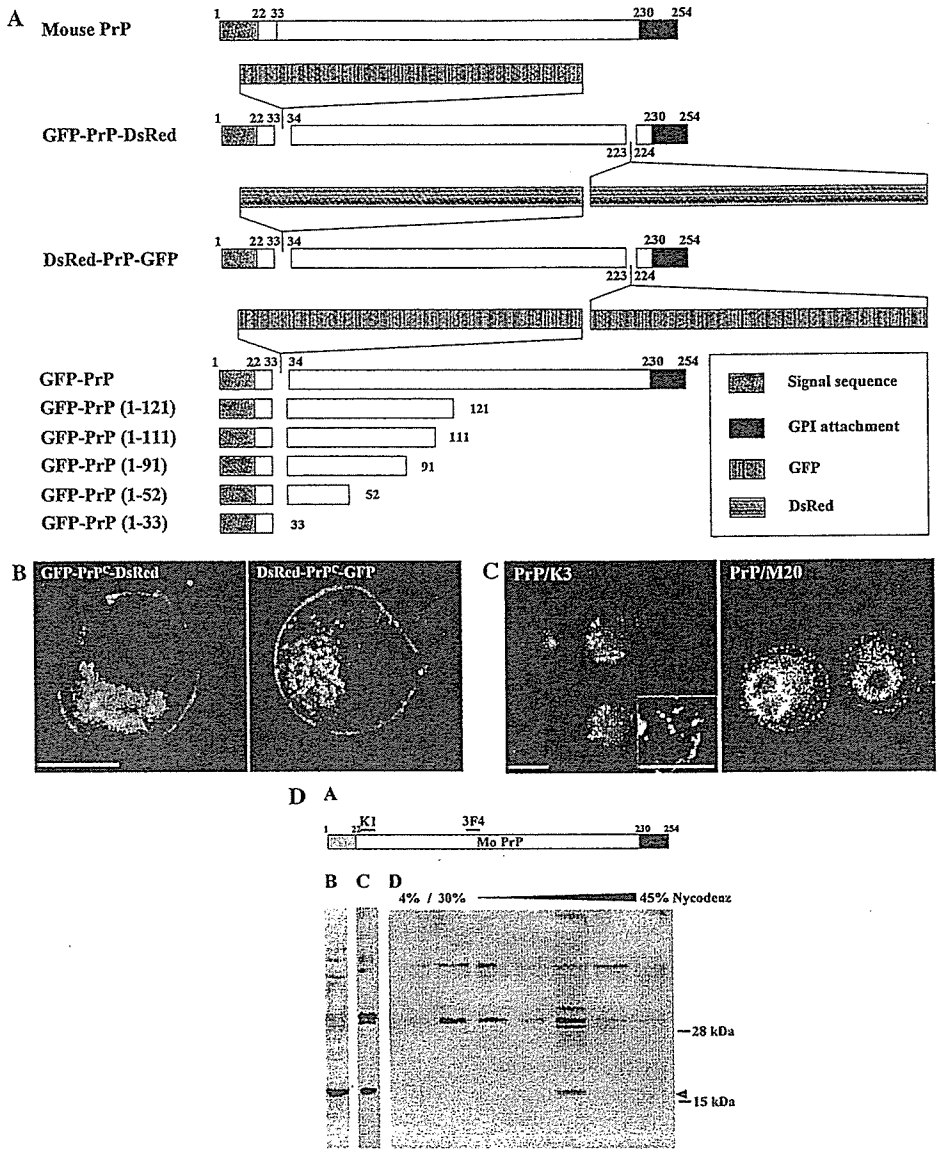

Fig. 1. Immunofluorescent analysis of fluorescent PrP^C. (A) The chimeric fluorescent PrP constructs (GFP–PrP–DsRed, DsRed–PrP–GFP, and the deletion mutant series,) used in this study. (B) Distribution patterns of GFP–PrP–DsRed (left panel): GFP–PrP^C (green) predominantly in the intracellular vesicles, PrP^C–DsRed (red) mostly at the cell surface membranes, and GFP–PrP^C–DsRed (yellow) in intracellular compartments. The DsRed–PrP–GFP (right panel) exhibits an inverted color profile indicating the same distribution patterns independent of the fluorescent conjugates. Scale bar = 8 μm. (C) Endogenous PrP^C is immunostained with anti-PrP polyclonal antibody K3 at a dilution of 1:200 (left panel) or M20 at a dilution of 1:200 (right panel). N2a cells were permeabilized with 0.1% Triton X-100. A distinct proportion of PrP^C is detected in a dot-like distribution pattern (an arrow). Scale bars = 15 μm. (D) 3F4 detects NH_2-terminal MHM2 PrP^C fragment of 17 kDa (arrow head) which was transiently transfected in N2a cells. To separate non-lipid raft fractions which contain high density, Triton X-100-insoluble intracellular membranes, we used the procedure of Naslavsky et al. [33] with slight modifications as below. Cells were lysed and resuspended in ice-cold buffer A (25 mM Hepes–KOH, pH 7.5, 5 mM EDTA, and 0.15 M NaCl) containing 1% Triton X-100, and then adjusted to 50% Nycodenz containing buffer A. Samples were centrifuged at 200,000*g* at 4 °C for 4 h by floatation in 1.5 ml of a discontinuous Nycodenz gradient (4/30/32.5/35/37.5/40/42.5/45%). After the centrifugation, samples were fractionated by 0.2 ml from the top of gradients.

PrP^C fragment contains at least residues 26–40, 76–90, and 108/111 in Mo PrP.

Microtubules-dependent intracellular localization of fluorescent PrP^C

These observations of the intracellular NH_2-terminal PrP^C fragment in a dot-like distribution pattern prompted us to further investigate its possible association with cytoskeletal proteins such as microtubules or actin. Co-immunostaining of endogenous PrP^C and microtubules by anti-PrP polyclonal antibody K3/anti-tubulin monoclonal antibody DM1A detected PrP^C along microtubules in N2a cells (Fig. 2) as well as HpL3-4 cells (data not shown). Subsequently, an immunoprecipitation assay performed with anti-tubulin antibody

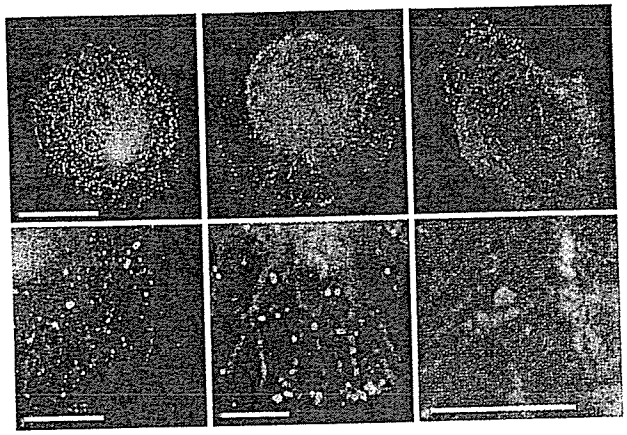

Fig. 2. Co-immunostaining of endogenous PrP^C and microtubules by anti-PrP antibody K3 (1:200, green) and anti-tubulin antibody DM1A (1:200, red) detects PrP^C along microtubules in N2a cells. Scale bar (upper panels) = 7 μm and scale bars (lower panels) = 3 μm.

(DM1A) resulted in the co-immunoprecipitation of tubulin and the NH_2-terminal PrP^C fragment of 17 kDa in N2a cells (Fig. 3A). Another polyclonal antibody K9 against the COOH-terminal residues 196–210 in Mo PrP failed to detect COOH-terminal PrP^C in the immunoprecipitated complex (Fig. 3A).

After N2a cells (Fig. 3B) were treated with 30 μM nocodazole which depolymerizes microtubules, the signals of GFP–PrP^C were congregated in a time-dependent manner. On the other hand, latrunculin A, which is widely used as an agent to sequester monomeric actin in living cells, did not affect the localization of GFP–PrP^C (data not shown). Finally, the deletion mutants (Fig. 1A) were used to map the amino acid residues responsible for the microtubules-associated localization of GFP–PrP^C. As shown in Fig. 3C, truncated constructs with the amino acid residues 1–121, 1–111, and 1–91 in Mo PrP exhibited its proper localization, whereas those with amino acid residues 1–52 and 1–33 in Mo PrP lost the dot-like distribution pattern.

Discussion

First of all, our double-labeled fluorescent PrP^C detected the NH_2-terminal and COOH-terminal PrP^C fragments with distinct subcellular distribution profiles, in which cleavage of PrP^C at around a middle region was involved [7,19,20].

Initial studies performed on the internalization of PrP^C using a chicken PrP^C have determined that endocytosis of chicken PrP is mediated by clathrin-coated pits, and the NH_2-terminal half of the chicken PrP polypeptide is essential for its endocytosis [21,22]. Recently, Nunziante et al. [23] also reported that the

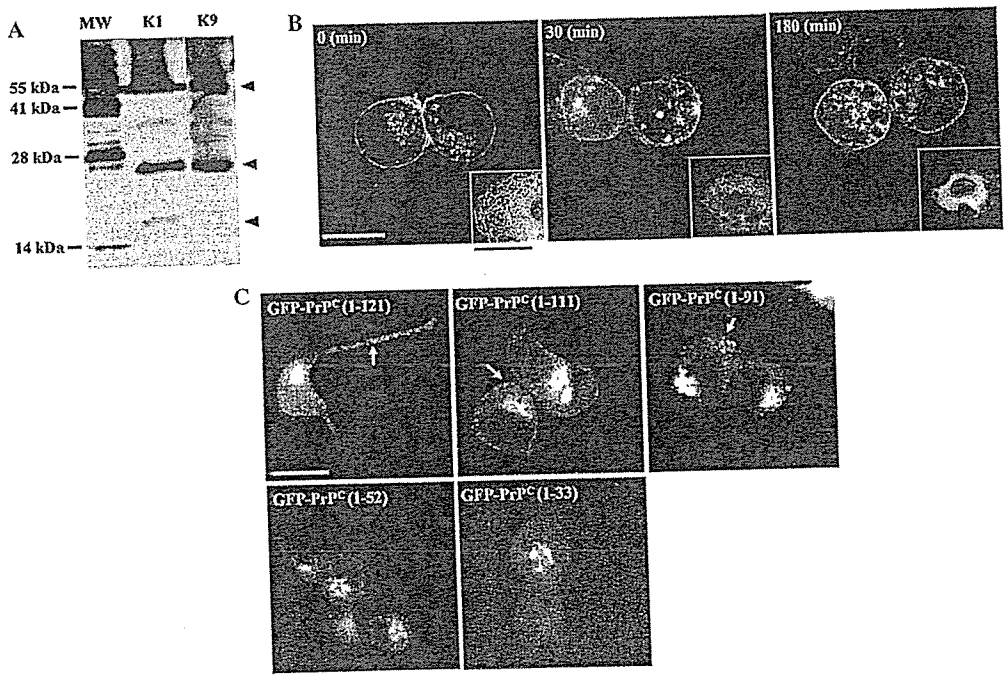

Fig. 3. The association of intracellular GFP–PrP^C with microtubules. (A) Co-immunoprecipitation of tubulin and the NH_2-terminal PrP^C fragment. Anti-tubulin antibody DM1A is used for the immunoprecipitation, and a polyclonal antibody K1 (1:500) against PrP residues 26–40 but not K9 (1:500) against residues 196–210 detects the NH_2-terminal PrP^C fragment of 17 kDa (lower arrow head) in the immunoprecipitated complex. Both K1 and K9 detect full length PrP^C (middle arrow head) and DM1A (1:2000) detects tubulin (upper arrow head). (B) After N2a cells were treated with 33 μM nocodazole and permeabilized with 0.1% Triton X-100, signals of GFP–PrP^C congregate in a time-dependent manner (0–180 min). Panels at the lower right corners represent depolymerized microtubules stained with anti-tubulin antibody DM1A (1:200). Scale bars = 15 μm. (C) The truncated GFP–PrP constructs with the amino acid residues 1–121, 1–111, and 1–91 in Mo PrP exhibit its proper localization (arrows), whereas those with 1–52 and 1–33 lose its dot-like distribution pattern. Scale bar = 15 μm.

N-proximal domain of the PrP functions as a putative targeting element and is essential for both transport to the plasma membrane and modulation of endocytosis. Along with these observations, GFP-tagged version of PrP^C was found to be properly anchored at the cell surface and its distribution pattern was similar to that of the endogenous PrP^C, with labeling at the plasma membrane and in an intracellular perinuclear compartment [10]. Further investigation concluded that PrP^C internalizes via a dynamin-dependent endocytic pathway and that the protein is targeted to the recycling endosomal compartment via Rab5-positive early endosomes and thus, traffic of GFP–PrP^C is delivered to classic endosomes after internalization [17]. Under our culture conditions, however, we could not demonstrate co-localization of the NH_2-terminal PrP^C fragment with any single specific organelle so far examined.

With this background, we have shown the microtubules-dependent intracellular localization of the NH_2-terminal PrP^C fragment in the cells. However, the question how intracellular PrP^C actually interacts with microtubules still remains to be examined. After internalized, the NH_2-terminal PrP^C fragment seems to reside inside vesicles where integral membrane proteins and linker proteins in some cases, for example, Jun kinase-interacting proteins (JIPs) [24,25], would be required for the interaction with microtubules to bridge the luminal and cytoplasmic phases across the membranes [26]. So far, we have not identified such intervening molecule/s involved in the PrP^C–microtubule interaction. Alternatively, a transmembrane form of PrP^C may be engaged in the direct interaction with the microtubules. It was suggested that a transmembrane form of PrP^C, termed C-transmembrane (^{ctm}PrP), has the COOH-terminus in the lumen with the NH_2-terminus accessible to proteases in the cytosol produced neurodegenerative changes in mice similar to those of some genetic prion diseases [27]. Such ^{ctm}PrP exposes its NH_2-terminus to the cytosol where the ^{ctm}PrP–microtubule interactions could theoretically occur, although it is less likely, as such transmembrane ^{ctm}PrP is rather pathogenic than physiologic. The fact that the truncated PrP^C with residues 1–91 cannot form ^{ctm}PrP [27], but still exhibits the microtubules-associated intracellular localization, also does not support the notion. Interestingly, these residues 1–91 partly overlap with an octapeptide repeat region, which is related to the copper metabolism [28–32]. Finally, it is also indispensable for identifying how many NH_2-terminal PrP^C fragments reside in each dot-like vesicle.

In summary, we demonstrated the microtubules-associated intracellular localization of NH_2-terminal PrP^C fragment at a steady state level. At the same time, a real time imaging analysis of fluorescent PrP^C in living cells has yet to be done toward further understanding of its mode of existence and dynamics along the microtubular network.

Acknowledgments

We greatly thank S.B. Prusiner and D.A. Harris for discussions and comments, T. Onodera for providing us the HpL3-4 cell line, M. Kawabata, E. Nannri, C. Ota, and Y. Yamaura for technical assistances. This work was supported by grants from the Core Research for Evolutional Science and Technology (CREST) of Japan Science and Technology Agency, Health and Labour Sciences Research Grants, Research on Advanced Medical Technology, nano-001, and the Ministry of Health, Labor, and Welfare of Japan.

References

[1] C. Kuwahara, A.M. Takeuchi, T. Nishimura, K. Haraguchi, A. Kubosaki, Y. Matsumoto, K. Saeki, T. Yokoyama, S. Itohara, T. Onodera, Prions prevent neuronal cell-line death, Nature 400 (1999) 225–226.
[2] S.B. Prusiner, Prions, Proc. Natl. Acad. Sci. USA 95 (1998) 13363–13383.
[3] S.B. Prusiner, D.C. Bolton, D.F. Groth, K.A. Bowman, S.P. Cochran, M.P. McKinley, Further purification and characterization of scrapie prions, Biochemistry 21 (1982) 6942–6950.
[4] S.B. Prusiner, P. Peters, K. Kaneko, A. Taraboulos, V. Lingappa, F.E. Cohen, S.J. DeArmond, Cell biology of prions, in: S.B. Prusiner (Ed.), Prion Biology and Diseases, Cold Spring Harbor, New York, 1999, pp. 349–391, Chap. 9.
[5] N. Stahl, D.R. Borchelt, K. Hsiao, S.B. Prusiner, Scrapie prion protein contains a phosphatidylinositol glycolipid, Cell 51 (1987) 229–240.
[6] B. Caughey, R.E. Race, D. Ernst, M.J. Buchmeier, B. Chesebro, Prion protein biosynthesis in scrapie-infected and uninfected neuroblastoma cells, J. Virol. 63 (1989) 175–181.
[7] A. Taraboulos, M. Scott, A. Semenov, D. Avrahami, L. Laszlo, S.B. Prusiner, Cholesterol depletion and modification of COOH-terminal targeting sequence of the prion protein inhibit formation of the scrapie isoform, J. Cell Biol. 129 (1995) 121–132.
[8] M. Vey, S. Pilkuhn, H. Wille, R. Nixon, S.J. DeArmond, E.J. Smart, R.G. Anderson, A. Taraboulos, S.B. Prusiner, Subcellular colocalization of the cellular and scrapie prion proteins in caveolae-like membranous domains, Proc. Natl. Acad. Sci. USA 93 (1996) 14945–14949.
[9] K. Kaneko, M. Vey, M. Scott, S. Pilkuhn, F.E. Cohen, S.B. Prusiner, COOH-terminal sequence of the cellular prion protein directs subcellular trafficking and controls conversion into the scrapie isoform, Proc. Natl. Acad. Sci. USA 94 (1997) 2333–2338.
[10] K.S. Lee, A.C. Magalhaes, S.M. Zanata, R.R. Brentani, V.R. Martins, M.A. Prado, Internalization of mammalian fluorescent cellular prion protein and N-terminal deletion mutants in living cells, J. Neurochem. 79 (2001) 79–87.
[11] L. Ivanova, S. Barmada, T. Kummer, D.A. Harris, Mutant prion proteins are partially retained in the endoplasmic reticulum, J. Biol. Chem. 276 (2001) 42409–42421.
[12] A. Negro, C. Ballarin, A. Bertoli, M.L. Massimino, M.C. Sorgato, The metabolism and imaging in live cells of the bovine prion protein in its native form or carrying single amino acid substitutions, Mol. Cell Neurosci. 17 (2001) 521–538.
[13] H. Lorenz, O. Windl, H.A. Kretzschmar, Cellular phenotyping of secretory and nuclear prion proteins associated with inherited prion diseases, J. Biol. Chem. 277 (2002) 8508–8516.
[14] D.A. Butler, M.A. Scott, J.M. Bockman, D.R. Borchelt, A. Taraboulos, K.K. Hsiao, D.T. Kingsbury, S.B. Prusiner, Scrapie-

infected murine neuroblastoma cells produce protease-resistant prion proteins, J. Virol. 62 (1988) 1558–1564.
[15] M.R. Scott, R. Kohler, D. Foster, S.B. Prusiner, Chimeric prion protein expression in cultured cells and transgenic mice, Protein Sci. 1 (1992) 986–997.
[16] T.A. Schroer, M.P. Sheetz, Role of kinesin and kinesin-associated proteins in organelle transport, in: F.D. Warner, J.R. McIntosh (Eds.), Cell Movement, Alan R. Liss, New York, 1989, pp. 295–306.
[17] A.C. Magalhaes, J.A. Silva, K.S. Lee, V.R. Martins, V.F. Prado, S.S.G. Ferguson, M.V. Gomez, R.R. Brentani, M.A.M. Prado, Endocytic intermediates involved with the intracellular trafficking of a fluorescent cellular prion protein, J. Biol. Chem. 277 (2002) 33311–33318.
[18] R.J. Kascsak, R. Rubenstein, P.A. Merz, M. Tonna-DeMasi, R. Fersko, R.I. Carp, H.M. Wisniewski, H. Diringer, Mouse polyclonal and monoclonal antibody to scrapie-associated fibril proteins, J. Virol. 61 (1987) 3688–3693.
[19] M. Rogers, D. Serban, T. Gyuris, M. Scott, T. Torchia, S.B. Prusiner, Epitope mapping of the Syrian hamster prion protein utilizing chimeric and mutant genes in a vaccinia virus expression system, J. Immunol. 147 (1991) 3568–3574.
[20] K.-M. Pan, N. Stahl, S.B. Prusiner, Purification and properties of the cellular prion protein from Syrian hamster brain, Protein Sci. 1 (1992) 1343–1352.
[21] S.-L. Shyng, J.E. Heuser, D.A. Harris, A glycolipid-anchored prion protein is endocytosed via clathrin-coated pits, J. Cell Biol. 125 (1994) 1239–1250.
[22] S.-L. Shyng, K.L. Moulder, A. Lesko, D.A. Harris, The N-terminal domain of a glycolipid-anchored prion protein is essential for its endocytosis via clathrin-coated pits, J. Biol. Chem. 270 (1995) 14793–14800.
[23] M. Nunziante, S. Gilch, H.M. Schatzl, Essential role of the prion protein N terminus in subcellular trafficking and half-life of cellular prion protein, J. Biol. Chem. 278 (2003) 3726–3734.
[24] A.B. Bowman, A. Kamal, B.W. Ritchings, A.V. Philp, M. McGrail, J.G. Gindhart, L.S. Goldstein, Kinesin-dependent axonal transport is mediated by the sunday driver (SYD) protein, Cell 103 (2000) 583–594.
[25] K.J. Verhey, D. Meyer, R. Deehan, J. Blenis, B.J. Schnapp, T.A. Rapoport, B. Margolis, Cargo of kinesin identified as JIP scaffolding proteins and associated signaling molecules, J. Cell Biol. 152 (2001) 959–970.
[26] M. Schliwa, G. Woehlke, Molecular motors, Nature 422 (2003) 759–765.
[27] R.S. Hegde, J.A. Mastrianni, M.R. Scott, K.A. DeFea, P. Tremblay, M. Torchia, S.J. DeArmond, S.B. Prusiner, V.R. Lingappa, A transmembrane form of the prion protein in neurodegenerative disease, Science 279 (1998) 827–834.
[28] D.R. Brown, K. Qin, J.W. Herms, A. Madlung, J. Manson, R. Strome, P.E. Fraser, T. Kruck, A. von Bohlen, W. Schulz-Schaeffer, A. Giese, D. Westaway, H. Kretzschmar, The cellular prion protein binds copper in vivo, Nature 390 (1997) 684–687.
[29] P.C. Pauly, D.A. Harris, Copper stimulates endocytosis of the prion protein, J. Biol. Chem. 273 (1998) 33107–33110.
[30] M.L. Kramer, H.D. Kratzin, B. Schmidt, A. Romer, O. Windl, S. Liemann, S. Hornemann, H. Kretzschmar, Prion protein binds copper within the physiological concentration range, J. Biol. Chem. 276 (2001) 16711–16719.
[31] W.S. Perera, N.M. Hooper, Ablation of the metal ion-induced endocytosis of the prion protein by disease-associated mutation of the octarepeat region, Curr. Biol. 11 (2001) 519–523.
[32] A.P. Garnett, J.H. Viles, Copper binding to the octarepeats of the prion protein. Affinity, specificity, folding, and cooperativity: insights from circular dichroism, J. Biol. Chem. 278 (2003) 6795–6802.
[33] N. Naslavsky, R. Stein, A. Yanai, G. Friedlander, A. Taraboulos, Characterization of detergent-insoluble complexes containing the cellular prion protein and its scrapie isoform, J. Biol. Chem. 272 (1997) 6324–6331.

Available online at www.sciencedirect.com
SCIENCE DIRECT®
Biochemical and Biophysical Research Communications 315 (2004) 802–807
BBRC
www.elsevier.com/locate/ybbrc

Anterograde and retrograde intracellular trafficking of fluorescent cellular prion protein

Naomi S. Hachiya, Kota Watanabe, Makiko Yamada, Yuji Sakasegawa, and Kiyotoshi Kaneko*

Department of Cortical Function Disorders, National Institute of Neuroscience (NIN), National Center of Neurology and Psychiatry (NCNP), and Core Research for Evolutional Science and Technology (CREST), Japan Science and Technology Agency, Tokyo 187-8502, Japan

Received 22 January 2004

Abstract

In order to investigate the microtubule-associated intracellular trafficking of the NH2-terminal cellular prion protein (PrP^C) fragment [Biochem. Biophys. Res. Commun. 313 (2004) 818], we performed a real-time imaging of fluorescent PrP^C (GFP-PrP^C) in living cells. Such GFP-PrP^C exhibited an anterograde movement towards the direction of plasma membranes at a speed of 140–180 nm/s, and a retrograde movement inwardly at a speed of 1.0–1.2 μm/s. The anterograde and retrograde movements of GFP-PrP^C were blocked by a kinesin family inhibitor (AMP-PNP) and a dynein family inhibitor (vanadate), respectively. Furthermore, anti-kinesin antibody (α-kinesin) blocked its anterograde motility, whereas anti-dynein antibody (α-dynein) blocked its retrograde motility. These data suggested the kinesin family-driven anterograde and the dynein-driven retrograde movements of GFP-PrP^C. Mapping of the interacting domains of PrP^C identified amino acid residues indispensable for interactions with kinesin family: NH2-terminal mouse (Mo) residues 53–91 and dynein: NH2-terminal Mo residues 23–33, respectively. Our findings argue that the discrete N-terminal amino acid residues are indispensable for the anterograde and retrograde intracellular movements of PrP^C.

Keywords: Cellular prion protein; Green fluorescent protein; Microtubules; Kinesin family; Dynein

The posttranslational conformational change of the cellular isoform of prion protein (PrP^C) into the scrapie isoform of prion protein (PrP^{Sc}) is the fundamental process underlying the pathogenesis of the prion disease [2,3]. An initial degradation of PrP^C involves cleavage of the NH2-terminal fragment to produce a COOH-terminal 17-kDa polypeptide which was found in a Triton X-100 insoluble fraction [4], of which the cleavage site was mapped at the amino acid residues between the 3F4 (amino acids 108/111 in mouse (Mo) PrP) and the 13A5 (amino acids 138 in Mo PrP) epitopes [4–6]. Several groups reported that NH2-terminal fragment of the PrP functions as a putative targeting element [7,8] and is essential for both transport to the plasma membrane and modulation of endocytosis [9]. GFP-tagged version of PrP^C was found to be properly anchored at the cell surface and its distribution pattern was similar to that of the endogenous PrP^C, with labelling at the plasma membrane and in an intracellular perinuclear compartment [10–14].

We previously demonstrated the microtubule-associated intracellular localization of the NH2-terminal fluorescent PrP^C fragment [1] in Mo neuroblastoma neuro2a (N2a), known to be infectable with PrP^{Sc} [15] and HpL3-4 cells, a hippocampal cell line established from *prnp* gene-ablated mice [16], by utilizing double-labelled PrP^C. At a steady state level, we detected NH_2-terminally fluorescent-tagged PrP^C predominantly in the intracellular compartments, COOH-terminally fluorescent-tagged PrP^C mostly at the cell surface membranes overlapping with lipid rafts, and PrP^C in full length with the merged color in Golgi compartments. The NH_2-terminal PrP^C fragment, which may not reflect the distribution to any single specific organelle, congregated in the cytosol after the treatment with a microtubule

* Corresponding author. Fax: +81-42-346-1748.
E-mail address: kaneko@ncnp.go.jp (K. Kaneko).

0006-291X/$ - see front matter © 2004 Elsevier Inc. All rights reserved.
doi:10.1016/j.bbrc.2004.01.126

depolymerizer (nocodazole). Such microtubule-associated intracellular localization required at least the 1–91 amino acid residues of the NH2-terminal PrP^C fragment.

With this background, we performed a follow-up study of intracellular GFP-PrP^C by a real-time imaging, which demonstrated the anterograde and retrograde intracellular movements of the NH_2-terminal PrP^C fragment in N2a and HpL3-4 cells.

Materials and methods

Construction of GFP-PrP and the deletion mutants. GFP-PrP constructs were made as previously described [1], and the resulted plasmid was designated pSPOX-MHM2PrP::GFP. The series of deletion mutants were amplified by PCR from the pSPOX-MHM2PrP::GFP [1] using 5′-GCA ACC GTT ACC CAC CTC AGG GGG GTA CCC ATA ATC AGT GGA ACA AGC CC-3′ as the forward primer and the following backward primers: 5′-CTG AGG TGG GTA ACG GTT GCC TCC AGG GCT-3′ (for amino acid residues Δ53–91 in Mo PrP), 5′-CTG ATG TCG GCC TCT GCA AAG GTA TGG TGA GC-3′ and 5′-TTT GCA GAG GCC GAC ATC AGT CCA CAT AGT-3′ (Δ23–33), digested with *Bam*HI and *Xho*I, and replaced with the *Bam*HI–*Xho*I fragment of pSPOX-MHM2PrP::GFP [17]. The resulted plasmids were verified by direct DNA sequencing.

Antibodies and drugs. Anti-kinesin and anti-dynein antibodies were purchased from Santa Cruz Biotechnology, and anti-γ-tubulin antibody was purchased from Sigma. Vanadate and AMP-PNP were purchased from CHEMICON and Sigma, respectively. Nocodazole was purchased from Sigma.

Cell cultures, DNA transfection, and drug treatments. Mo neuroblastoma neuro2a (N2a) cells known to be infectable with PrP^{Sc} [15] were obtained from American Tissue Culture Collection. A hippocampal cell line established from *prnp* gene-ablated mice (HpL3-4) was kindly provided by Dr. T. Onodera. Cells were grown and maintained at 37 °C in MEM supplemented with 10% fetal bovine serum. N2a and HpL3-4 cells were transiently transfected with each construct using a DNA transfection kit (Lipofectamin, Gibco-BRL). Western blot analyses were performed as described [17]. Vanadate (10 μM at 30 °C for 30 min) and AMP-PNP (100 μM and 2 mM at 30 °C for 30 min) treatments were performed according to the previous report [18].

Immunofluorescent microscopy. For indirect immunofluorescence analysis, fluorescent PrP^C-transfected N2a cells were rinsed with PBS with Ca^{2+} and Mg^{2+} (PBS(+)) and then fixed with 10% formalin in 70% PBS(+) for 30 min at room temperature. After four washes with PBS(−), the fixed cells were incubated 10% FBS in PBS(−) for 30 min at room temperature. They were then incubated for 1 h at room temperature with antibodies at desired concentrations. After four washes with PBS(−), the cells were incubated with either Alexa488 (green) Fluor-conjugated anti-rabbit IgG (Molecular Probes) or Alexa594 (red) Fluor-conjugated anti-mouse IgG (Molecular Probes), diluted 1:200 in PBS, for 1 h at room temperature. The stained cells were washed four times with PBS(−) and mounted with SLOW FADE (Molecular Probes). Samples were imaged with Delta-Vision microscopy system (Applied Precision), out of focus light of the visualized images was removed by interactive deconvolution.

Real-time imaging. To observe living cells, cells were cultured on glass-bottomed dishes (Matsunami) in culture medium without phenol red at 30 °C. Images of cells were collected with a Delta Vision Microscopy System (Applied Precision) equipped with an Olympus IX70 through a cooled CCD camera (Quantix-LC, Photometrics). Fluorescence signals were visualized using a quad beam splitter (Chroma) and the following excitation and emission filter 525/50 nm (Chroma).

In vitro motility assay. For cytosol preparations, N2a cells were collected from 9 cm × 10 dishes, washed and suspended in four volumes of PBS, homogenized, and ultracentrifuged. After ultracentrifugation at 100,000*g* for 60 min, supernatants were collected and used for these experiments. Alexa 594-labelled tubulin (Molecular Probe) was polymerized in PEM buffer (35 mM Pipes, pH 7.0, 0.5 mM EGTA, and 0.5 mM $MgCl_2$). Polymerized tubulin, recombinant GFP-PrP, and cytosol (1 mg/ml) were mixed and incubated at 30 °C for 5 min in PEM buffer in the presence of 1 mM ATP. After incubation, samples were spread onto glass-bottom dishes and then observed with the Delta Vision Microscopy System (Applied Precision).

Results

The intracellular trafficking of fluorescent PrP^C was investigated through the real-time imaging in living cells

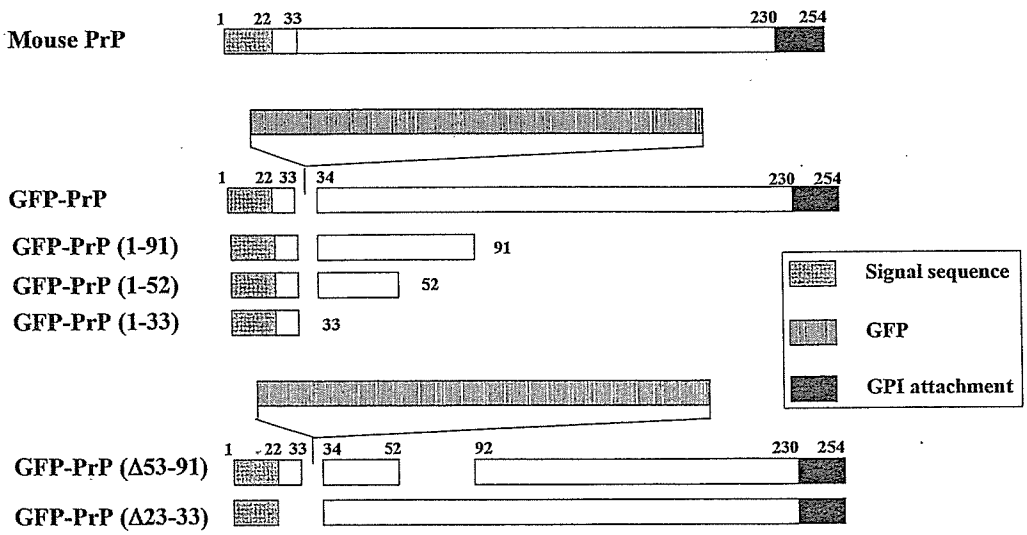

Fig. 1. Immunofluorescent analysis of GFP-PrP^C. The chimeric GFP-PrP constructs including the deletion mutant series used in this study. GFP-PrP (1–91), (1–52), and (1–33) constructs were made as previously described [1]. These recombinant GFP-PrPs were transfected in N2a cells.

by utilizing GFP-PrP constructs (Fig. 1). As results, we revealed that GFP-PrP^C transfected in N2a cells exhibited an anterograde movement towards the direction of plasma membranes at a speed of 140–180 nm/s as well as a retrograde movement inwardly at a speed of 1.0–1.2 μm/s (Fig. 2A). The same results were obtained from other experiments with GFP-PrP^C transfected in HpL3-4 cells (data not shown).

A kinesin family inhibitor of AMP-PNP at a concentration of 100 μM inhibited the anterograde movement of GFP-PrP^C which congregated at an intracellular perinuclear compartment (Fig. 2B), whereas a dynein family inhibitor of vanadate at a concentration of 10 μM inhibited the retrograde movement of GFP-PrP^C which was subsequently detected at the plasma membrane (Fig. 2B) [18]. At a concentration of 2 mM, AMP-PNP inhibited both kinesin and dynein families, and the intracellular motility of GFP-PrP^C was completely blocked (Fig. 2B). The intracellular trafficking of the NH_2-terminal PrP^C fragment was also blocked by the treatment with a microtubule depolymerizer (nocodazole) (data not shown). Furthermore, anti-kinesin antibody (α-kinesin) blocked the anterograde motility of GFP-PrP^C to congregate in an intracellular perinuclear compartment, and anti-dynein antibody (α-dynein) blocked its retrograde motility to reside at a plasma membrane (Fig. 2C).

Next, the deletion mutants (Fig. 1) were used to identify the amino acid residues responsible for the anterograde and retrograde movements of GFP-PrP^C. Truncated constructs with the amino acid residues 1–121, 1–111, and 1–91 in Mo PrP transfected in N2a cells

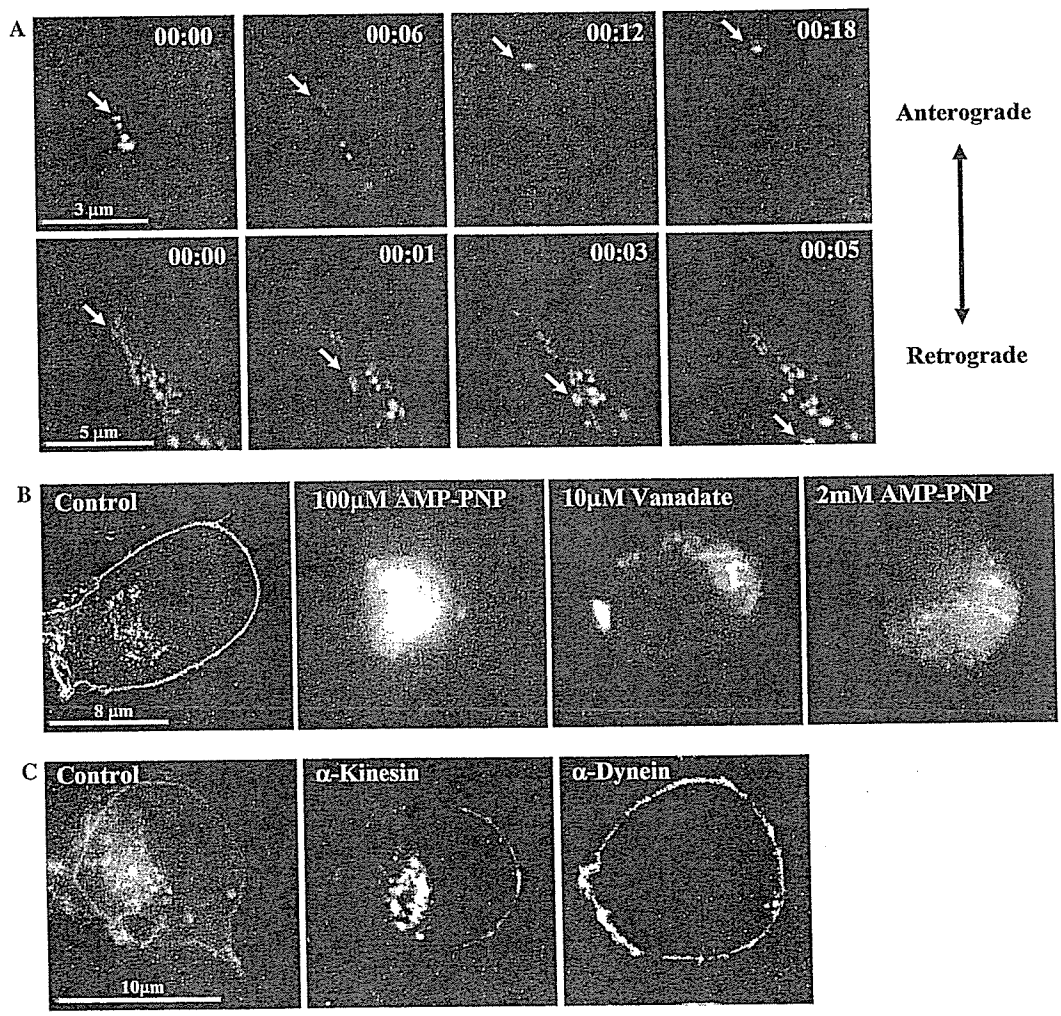

Fig. 2. Intracellular trafficking of GFP-PrP^C by a real-time imaging in living cells, and the drug- or antibody-mediated inhibitions of intracellular movements. (A) Recombinant GFP-PrP^C transfected in N2a cells exhibits an anterograde movement at a speed of 140–180 nm/s (upper panels) and an inward retrograde movement at a speed of 1.0–1.2 μm/s (lower panels). Scale bar (upper panel) = 3 μm and scale bar (lower panel) = 5 μm. (B) A kinesin family inhibitor of AMP-PNP at a concentration of 100 μM inhibited the anterograde movement of GFP-PrP^C which congregates in an intracellular perinuclear compartment. A dynein family inhibitor of vanadate at a concentration of 10 μM inhibits the retrograde movement of GFP-PrP^C which congregates at a plasma membrane. At a concentration of 2 mM, AMP-PNP inhibits both kinesin and dynein families, and the intracellular motility of GFP-PrP^C is completely blocked. Scale bar = 8 μm. (C) Anti-kinesin antibody (α-kinesin) blocks the anterograde motility of GFP-PrP^C and anti-dynein antibody (α-dynein) blocks its retrograde motility.

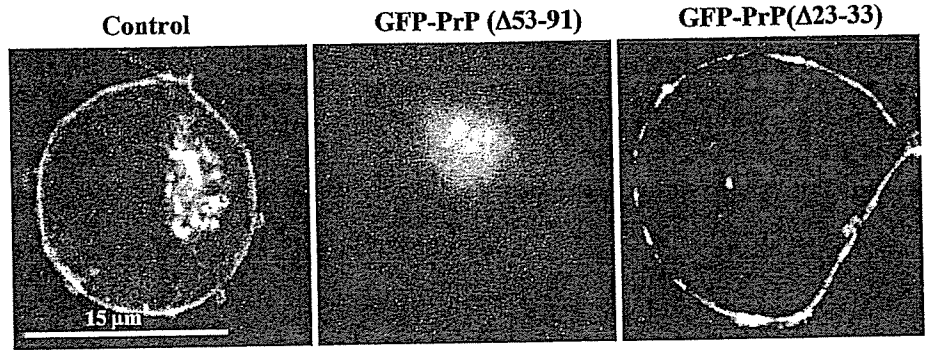

Fig. 3. The amino acid residues responsible for the anterograde and retrograde movements of GFP-PrP^C. The truncated construct of GFP-PrP lacking the amino acid residues 53–91 in Mo PrP loses its anterograde motility and congregates in the intracellular perinuclear compartment. The GFP-PrP construct lacking the amino acid residues 23–33 in Mo PrP loses its retrograde motility and resides at the plasma membrane. Scale bar = 15 μm.

exhibited its proper anterograde and retrograde motilities (data not shown), whereas those with amino acid residues 1–52 and 1–33 in Mo PrP did not [1]. These truncated GFP-PrP^C (1–33 and 1–52) surrounded the γ-tubulin-positive centrosome (microtubule organizing center) (data not shown), suggesting that the truncated GFP-PrP^C with at most 1–52 lost its anterograde movement but those with at least 1–33 still exhibited the dynein-driven retrograde movement. Thus, discrete amino acid residues 53–91 and 23–33 (the first NH2-terminal 1–22 amino acid residues act as a signal sequence) seem to be indispensable for the anterograde and retrograde movements, respectively. In accordance with these observations, the deletion constructs lacking the amino acid residues 53–91 in Mo PrP (GFP-PrP^C (Δ53–91)) lost its anterograde motility and congregated in an intracellular perinuclear compartment, whereas those lacking the amino acid residues 23–33 (GFP-PrP^C (Δ23–33)) lost its retrograde motility and resided at a plasma membrane (Fig. 3).

Finally, an in vitro motility assay [19] was further performed to obtain direct evidence on the interaction at the cytosolic interface between recombinant GFP-PrP and Alexa 594-labelled microtubules with or without cytosolic fractions including kinesin family and dynein motor proteins. However, no movement of GFP-PrP along Alexa 594-labelled microtubules was observed even after the addition of cytosolic fractions (Fig. 4).

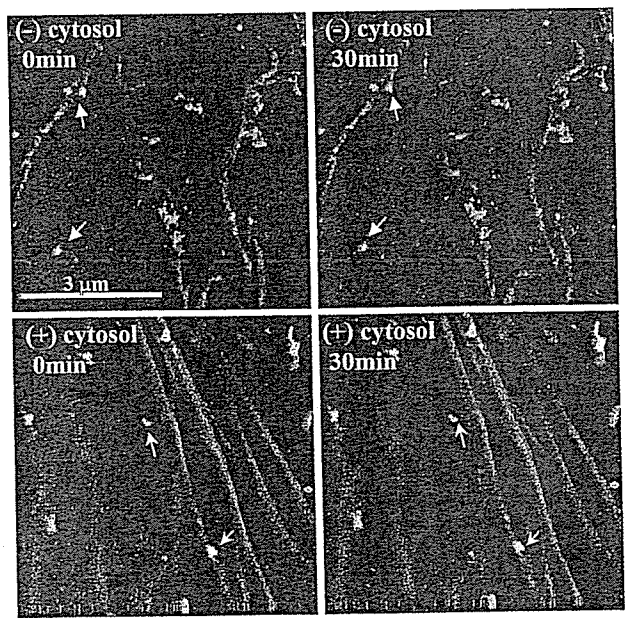

Fig. 4. In vitro motility assay of recombinant GFP-PrP. Polymerized Alexa 594-labelled tubulin, recombinant GFP-PrP, and cytosol (1 mg/ml) were incubated at 30 °C for 5 min in the presence of 1 mM ATP. No movement of recombinant GFP-PrP (arrow heads) along Alexa 594-labelled microtubules was observed for 0–30 min even after the addition of cytosolic fractions (cytosol). Scale bar = 3 μm.

Discussion

We previously reported the microtubule-associated intracellular localization of NH2-terminal PrP^C fragment at a steady state level [1]. A real-time imaging of GFP-PrP^C in living cells, however, has been awaited for further understanding its dynamics along the microtubular network.

Microtubules are essential and ubiquitous cytoskeletal elements composed of heterodimers of α- and β-tubulin, and serve many vital roles, participating in organization of the cytoplasm, in cell motility, and in mitosis [20,21]. In addition to tubulin itself, several microtubule-associated proteins (MAPs) comprise cellular microtubules. The molecular motors that move along microtubules have two origins. The kinesin and myosin families of ATPase motors share a common core structure and may have the same common ancestor as the GTPases involved in signalling and protein synthesis [20,22]. Dynein is part of the family of AAA ATPases [23] that also contribute to protein folding (Hsp100 chaperones), membrane traffic (*N*-ethylmaleimide-sensitive factor or NSF), and DNA synthesis (clamp loader proteins).

Here we showed the anterograde transport of GFP-PrP^C at a speed of 140–180 nm/s and the retrograde transport at a speed of 1.0–1.2 μm/s. These anterograde and retrograde transports of GFP-PrP^C were completely inhibited by AMP-PNP/vanadate which stop the kinesin family/dynein family-driven movements, respectively. Furthermore, anti-kinesin antibody (α-kinesin) blocked the anterograde motility of GFP-PrP^C, and anti-dynein antibody (α-dynein) blocked its retrograde motility. Among the kinesin superfamily, KIF4 moves latex beads from the minus to the plus ends of microtubules, a direction that corresponds to anterograde transport in the axon at a speed of <200 nm/s [24], and dynein is the force-generating protein that produces force in the direction corresponding to retrograde organelle transport at a speed of about 1.4 μm/s in the cell [25–28]. Thus, the anterograde transport of intracellular GFP-PrP^C might be compatible with the speed of the KIF4-driven movement, while the retrograde movement is compatible with that of the dynein-driven movement.

Mapping of the distinct kinesin family-interacting domain and the dynein-interacting domain identified the minimum required amino acid residues in the NH2-terminal PrP^C fragment. The kinesin family-interacting domain (Mo 53–91) is overlapped with an octapeptide repeat region, which is related to the copper metabolism [29–33]. In terms of the PrP^{Sc} formation, the C-terminal domain of PrP^C is known to be insufficient to impede the conversion of the full-length PrP^C molecule to PrP^{Sc} and N-terminally truncated molecules (with residues 23–88 and 23–120 deleted) have reduced dominant-negative activity, and the extreme N-terminal sequence (23KKRPKP29) enhances the dominant-negative phenotype on the formation of PrP^{Sc} [34,35]. This basic sequence is highly conserved in all species studied to date [36]. On the other hand, deletion of the octarepeat sequences (residues 52–91) did not alter PrP^{Sc} formation and dominant-negative inhibition on the formation of PrP^{Sc} [35]. The relevance of these observations to the intracellular trafficking of PrP^C needs to be further investigated.

After internalized, the NH2-terminal PrP^C fragment seems to reside inside vesicles where integral membrane proteins and linker proteins in some cases would be required for the interaction with microtubules to bridge the luminal and cytoplasmic phases across the membranes [1]. Thus, it seems less likely that PrP^C is engaged in the direct interaction with the motor molecules, which is compatible with the fact that the in vitro motility assay failed to show that recombinant GFP-PrP directly moved along Alexa 594-labelled microtubules.

It is also important to identify how many NH2-terminal PrP^C fragments reside in each PrP^C-positive vesicle. In order to answer this question, a single fluorescent molecule is a good potential source because it can emit only one photon at a time. Otherwise it is indispensable to utilize a technique which allows us to know how many photons emit from each PrP^C molecule. Unfortunately, we are currently unable to utilize these techniques. Nonetheless, our results shed a new right on the mechanisms underlying the intracellular trafficking of PrP^C.

Acknowledgments

We greatly thank T. Onodera for providing us the HpL3-4 cell line, E. Nannri, K. Ishibashi, C. Ota, and Y. Yamaura for technical assistance. This work was supported by grants from the Core Research for Evolutional Science and Technology (CREST) of Japan Science and Technology Corporation, Health and Labour Sciences Research Grants, Research on Advanced Medical Technology, nano-001, and the Ministry of Health, Labor and Welfare of Japan.

References

[1] N. Hachiya, K. Watanabe, Y. Sakasegawa, K. Kaneko, Microtubules-associated intracellular localization of the NH2-terminal cellular prion protein fragment, Biochem. Biophys. Res. Commun. 313 (2004) 818–823.
[2] S.B. Prusiner, D.C. Bolton, D.F. Groth, K.A. Bowman, S.P. Cochran, M.P. McKinley, Further purification and characterization of scrapie prions, Biochemistry 21 (1982) 6942–6950.
[3] S.B. Prusiner, P. Peters, K. Kaneko, A. Taraboulos, V. Lingappa, F.E. Cohen, S.J. DeArmond, Cell Biology of Prions, Cold Spring Harbor, New York, 1999.
[4] A. Taraboulos, M. Scott, A. Semenov, D. Avrahami, L. Laszlo, S.B. Prusiner, Cholesterol depletion and modification of COOH-terminal targeting sequence of the prion protein inhibit formation of the scrapie isoform, J. Cell Biol. 129 (1995) 121–132.
[5] M. Rogers, D. Serban, T. Gyuris, M. Scott, T. Torchia, S.B. Prusiner, Epitope mapping of the Syrian hamster prion protein utilizing chimeric and mutant genes in a vaccinia virus expression system, J. Immunol. 147 (1991) 3568–3574.
[6] K.-M. Pan, N. Stahl, S.B. Prusiner, Purification and properties of the cellular prion protein from Syrian hamster brain, Protein Sci. 1 (1992) 1343–1352.
[7] S.-L. Shyng, J.E. Heuser, D.A. Harris, A glycolipid-anchored prion protein is endocytosed via clathrin-coated pits, J. Cell Biol. 125 (1994) 1239–1250.
[8] S.-L. Shyng, K.L. Moulder, A. Lesko, D.A. Harris, The N-terminal domain of a glycolipid-anchored prion protein is essential for its endocytosis via clathrin-coated pits, J. Biol. Chem. 270 (1995) 14793–14800.
[9] M. Nunziante, S. Gilch, H.M. Schatzl, Essential role of the prion protein N terminus in subcellular trafficking and half-life of cellular prion protein, J. Biol. Chem. 278 (2003) 3726–3734.
[10] K.S. Lee, A.C. Magalhaes, S.M. Zanata, R.R. Brentani, V.R. Martins, M.A. Prado, Internalization of mammalian fluorescent cellular prion protein and N-terminal deletion mutants in living cells, J. Neurochem. 79 (2001) 79–87.
[11] A.C. Magalhaes, J.A. Silva, K.S. Lee, V.R. Martins, V.F. Prado, S.S.G. Ferguson, M.V. Gomez, R.R. Brentani, M.A.M. Prado, Endocytic intermediates involved with the intracellular trafficking of a fluorescent cellular prion protein, J. Biol. Chem. 277 (2002) 33311–33318.
[12] A. Negro, C. Ballarin, A. Bertoli, M.L. Massimino, M.C. Sorgato, The metabolism and imaging in live cells of the bovine prion

protein in its native form or carrying single amino acid substitutions, Mol. Cell. Neurosci. 17 (2001) 521–538.
[13] H. Lorenz, O. Windl, H.A. Kretzschmar, Cellular phenotyping of secretory and nuclear prion proteins associated with inherited prion diseases, J. Biol. Chem. 277 (2002) 8508–8516.
[14] L. Ivanova, S. Barmada, T. Kummer, D.A. Harris, Mutant prion proteins are partially retained in the endoplasmic reticulum, J. Biol. Chem. 276 (2001) 42409–42421.
[15] D.A. Butler, M.A. Scott, J.M. Bockman, D.R. Borchelt, A. Taraboulos, K.K. Hsiao, D.T. Kingsbury, S.B. Prusiner, Scrapie-infected murine neuroblastoma cells produce protease-resistant prion proteins, J. Virol. 62 (1988) 1558–1564.
[16] C. Kuwahara, A.M. Takeuchi, T. Nishimura, K. Haraguchi, A. Kubosaki, Y. Matsumoto, K. Saeki, T. Yokoyama, S. Itohara, T. Onodera, Prions prevent neuronal cell-line death, Nature 400 (1999) 225–226.
[17] M.R. Scott, R. Kohler, D. Foster, S.B. Prusiner, Chimeric prion protein expression in cultured cells and transgenic mice, Protein Sci. 1 (1992) 986–997.
[18] T.A. Schroer, M.P. Sheetz, Role of kinesin and kinesin-associated proteins in organelle transport, in: F.D. Warner, J.R. McIntosh (Eds.), Cell Movement, Alan R. Liss, New York, 1989, pp. 295–306.
[19] A. Kubo, H. Sasaki, A. Yuba-Kubo, S. Tsukita, N. Shiina, Centriolar satellites: molecular characterization, ATP-dependent movement toward centrioles and possible involvement in ciliogenesis, J. Cell Biol. 147 (1999) 969–980.
[20] T.D. Pollard, The cytoskeleton, cellular motility and the reductionist agenda, Nature 422 (2003) 741–745.
[21] J. Howard, A.A. Hyman, Dynamics and mechanics of the microtubule plus end, Nature 422 (2003) 753–758.
[22] R.D. Vale, R.A. Milligan, The way things move: looking under the hood of molecular motor proteins, Science 288 (2000) 88–95.
[23] G. Mocz, I.R. Gibbons, Model for the motor component of dynein heavy chain based on homology to the AAA family of oligomeric ATPases, Structure (Camb) 9 (2001) 93–103.
[24] N. Hirokawa, Kinesin and dynein superfamily proteins and the mechanism of organelle transport, Science 279 (1998) 519–526.
[25] R.D. Vale, B.J. Schnapp, T. Mitchison, E. Steuer, T.S. Reese, M.P. Sheetz, Different axoplasmic proteins generate movement in opposite directions along microtubules in vitro, Cell 43 (1985) 623–632.
[26] R.D. Vale, T.S. Reese, M.P. Sheetz, Identification of a novel force-generating protein, kinesin, involved in microtubule-based motility, Cell 42 (1985) 39–50.
[27] B.M. Paschal, R.B. Vallee, Retrograde transport by the microtubule-associated protein MAP 1C, Nature 330 (1987) 181–183.
[28] R.B. Vallee, J.S. Wall, B.M. Paschal, H.S. Shpetner, Microtubule-associated protein 1C from brain is a two-headed cytosolic dynein, Nature 332 (1988) 561–563.
[29] D.R. Brown, K. Qin, J.W. Herms, A. Madlung, J. Manson, R. Strome, P.E. Fraser, T. Kruck, A. von Bohlen, W. Schulz-Schaeffer, A. Giese, D. Westaway, H. Kretzschmar, The cellular prion protein binds copper in vivo, Nature 390 (1997) 684–687.
[30] P.C. Pauly, D.A. Harris, Copper stimulates endocytosis of the prion protein, J. Biol. Chem. 273 (1998) 33107–33110.
[31] M.L. Kramer, H.D. Kratzin, B. Schmidt, A. Romer, O. Windl, S. Liemann, S. Hornemann, H. Kretzschmar, Prion protein binds copper within the physiological concentration range, J. Biol. Chem. 276 (2001) 16711–16719.
[32] W.S. Perera, N.M. Hooper, Ablation of the metal ion-induced endocytosis of the prion protein by disease-associated mutation of the octarepeat region, Curr. Biol. 11 (2001) 519–523.
[33] A.P. Garnett, J.H. Viles, Copper binding to the octarepeats of the prion protein. Affinity, specificity, folding, and cooperativity: insights from circular dichroism, J. Biol. Chem. 278 (2003) 6795–6802.
[34] K. Kaneko, L. Zulianello, M. Scott, C.M. Cooper, A.C. Wallace, T.L. James, F.E. Cohen, S.B. Prusiner, Evidence for protein X binding to a discontinuous epitope on the cellular prion protein during scrapie prion propagation, Proc. Natl. Acad. Sci. USA 94 (1997) 10069–10074.
[35] L. Zulianello, K. Kaneko, M. Scott, S. Erpel, D. Han, F.E. Cohen, S.B. Prusiner, Dominant-negative inhibition of prion formation diminished by deletion mutagenesis of the prion protein [In Process Citation], J. Virol. 74 (2000) 4351–4360.
[36] P. Bamborough, H. Wille, G.C. Telling, F. Yehiely, S.B. Prusiner, F.E. Cohen, Prion protein structure and scrapie replication: theoretical, spectroscopic, and genetic investigations, Cold Spring Harb. Symp. Quant. Biol. 61 (1996) 495–509.

GLIA 47:68–77 (2004)

Heterogeneity and Potentiation of AMPA Type of Glutamate Receptors in Rat Cultured Microglia

YUKIKO HAGINO,[1] YUKIHIRO KARIURA,[1] YOSHIMASA MANAGO,[1] TAIJU AMANO,[1] BING WANG,[1] MASAYUKI SEKIGUCHI,[2] KAORI NISHIKAWA,[2] SHUNSUKE AOKI,[2] KEIJI WADA,[2] AND MAMI NODA[1]*

[1]*Laboratory of Pathophysiology, Graduate School of Pharmaceutical Sciences, Kyushu University, Fukuoka, Japan*

[2]*Department of Degenerative Neurological Diseases, National Institute of Neuroscience, National Center of Neurology and Psychiatry, Tokyo, Japan*

KEY WORDS whole-cell patch clamp; kainate; PEPA; cyclothiazide; flip; flop; RT-PCR; TNF-α

ABSTRACT α-amino-hydroxy-5-methyl-isoxazole-4-propionate (AMPA) receptor in rat cultured microglia were analyzed precisely using flop- and flip-preferring allosteric modulators of AMPA receptors, 4-[2-(phenylsulfonylamino)ethylthio]-2,6-difluoro-phenoxyacetamide (PEPA) and cyclothiazide (CTZ), respectively. Glutamate (Glu)- or kainite (KA)-induced currents were completely inhibited by a specific blocker of AMPA receptor, LY300164, indicating that functional Glu-receptors in cultured microglia are mostly AMPA receptor but not KA receptor in many cells. Glu- and KA-induced currents were potentiated by PEPA and CTZ in a concentration-dependent manner. The ratio of the potentiation by PEPA to the potentiation by cyclothiazide varied with cells between 0.1 and 0.9, suggesting cell-to-cell heterogeneity of AMPA receptor subunits expressed in microglia. Quantitative RT-PCR revealed that GluR1-3 mainly occurred in the flip forms, which agreed with the stronger potentiation of receptor currents by CTZ vs. PEPA. Finally, the potentiation of microglial AMPA receptors by PEPA and CTZ inhibited the Glu-induced release of tumor necrosis factor-α (TNF-α) unpredictably. The increase in TNF-α release by Glu or KA required extracellular Na^+ and Ca^{2+} ions but not mitogen-activated protein kinase (MAPK), suggesting the effects of PEPA and CTZ were not due to the inhibition of MAPK. These results suggest that potentiation of microglial AMPA receptors serves as a negative feedback mechanism for the regulation of TNF-α release and may contribute to the ameliorating effects of allosteric modulators of AMPA receptors.

INTRODUCTION

There is increasing evidence that functional glutamate (Glu) receptors are not restricted to neurons but also expressed in glial cells. Among glial cells, microglial cells express α-amino-hydroxy-5-methyl-isoxazole-4-propionate (AMPA)/kainite (KA) type of Glu receptors and the activation of Glu receptors triggered the release of tumor necrosis factor-α (TNF-α) from microglial cells (Noda et al., 2000). The neuron-glia interaction via Glu was proposed where microglia played an important role (Bezzi et al., 2001). Microglial cells are rapidly activated in response to even minor pathological changes so that they may be viewed as the cellular sensory element of brain pathology (Kreutzberg, 1996). Microglia likely contribute neurodegenerative diseases and dementia in AIDS (Streit

Grant sponsor: Grants-in-Aid for Scientific Research of Japan Society for Promotion of Science; Grant sponsor: Research Grant in Priority Area Research of the Ministry of Education, Culture, Sports, Science and Technology, Japan; Grant sponsor: Kyushu University Foundation; Grant sponsor: Grants-in-Aid for Scientific Research of the Ministry of Health, Labor and Welfare, Japan; Grant sponsor: the Organization for Pharmaceutical Safety and Research, Japan. Yukiko Hagino's present address is Daiichi Suntory Biomedical Research Limited, Osaka, Japan.

*Correspondence to: Mami Noda, Laboratory of Pathophysiology, Graduate School of Pharmaceutical Sciences, Kyushu University, Fukuoka 812-8582, Japan. E-mail: noda@phar.kyushu-u.ac.jp

Received 5 February 2003; Accepted 30 December 2003

DOI 10.1002/glia.20034

Published online 24 March 2004 in Wiley InterScience (www.interscience.wiley.com).

and Kincaid-Colton, 1995). Glu receptors in microglia may contribute to an important role especially in these pathological conditions. Therefore, detailed analyses on Glu receptor in microglia, for example, subunit composition and expression pattern, should be important for understanding the functional role of microglia.

Functional AMPA receptors are assembled tetramers (Sun et al., 2002) formed from subunits encoded by four different genes, GluR1, GluR2, GluR3, and GluR4 (Hollmann et al., 1989; Keinanen et al., 1990). Each subunit is known to exist as two isoforms, flip and flop, which are produced by alternative RNA splicing (Sommer et al., 1990). AMPA receptors consisting of different subunit and/or splice-variant combinations show different properties. For example, it has been found that incorporation of GluR2 into receptor complexes dramatically reduced calcium ion permeability of the receptor channel (Hollmann et al., 1991; Hume et al., 1991). Incorporation of differentially spliced isoforms into receptor complexes produces AMPA receptors with different desensitization profiles (Sommer et al., 1990; Mosbacher et al., 1994).

In the present study, we aimed to detect cell-to-cell heterogeneity of functional AMPA receptors in microglia by use of two allosteric potentiators of the receptors. One is 4-[2-(phenylsulfonylamino)ethylthio]-2,6-difluoro-phenoxyacetamide (PEPA), a flop-preferring modulator (Sekiguchi et al., 1997), and the other is cyclothiazide (CTZ), a flip-preferring modulator (Partin et al., 1994; Kessler et al., 2000). Both compounds suppress desensitization of AMPA receptors (Partin et al., 1996; Sekiguchi et al., 1997, 1998, 2002) and we already showed that cyclothiazide dramatically enhanced the AMPA receptor currents in microglia (Noda et al., 2000). Comparing the action of cyclothiazide with that of PEPA was an effective means for detecting flip/flop heterogeneity among AMPA receptors expressed in hippocampal neurons (Sekiguchi et al., 1998). Here, we show the heterogeneity of microglia based on the AMPA receptor expression.

In addition to the electrophysiological analyses, the effects of PEPA and cyclothiazide on the release of TNF-α from microglia were also investigated. We previously observed that Glu and KA stimulated TNF-α release from microglia (Noda et al., 2000). Surprisingly, potentiation of AMPA receptors by PEPA did not enhance TNF-α release from microglia but rather had opposite effects. These results suggest that the activation of AMPA receptors evoked complex signaling pathways to the TNF-α release event. Our data on the detection of heterogeneity and potentiation of AMPA receptors should be useful for further investigation on the functional role of microglia.

MATERIALS AND METHODS

Papain and DNase were purchased from Worthington Biochemical (Freehold, NJ). Eagle's medium (MEM) was obtained from Nissui (Tokyo, Japan). Fetal calf serum (FCS) was from Hyclone Laboratories (Logan, UT). KA, Glu, isolectin-B_4, and PD 098059 were purchased from Sigma Chemical (St. Louis, MO). CTZ and AMPA were from Tocris Cookson (Bristol, U.K.). PEPA was prepared as described previously (Sekiguchi et al., 1997, 1998) and LY300164 [7-acetyl-5-(4-aminophenyl)-8,9-dihydro-8-methyl-7H-1,3-dioxolo(4,5H)-2,3-benzodiazepine] was a gift from Eli Lilly (Surrey, U.K.).

Cell Culture

Microglial cells were isolated from the mixed cultures of cerebrocortical cells from postnatal day 3 Wistar rats (Kyudo, Kumamoto, Japan) as described previously (Noda et al., 1999). In brief, the cerebral cortex was minced and treated twice with papain (90 units) and DNase (2000 units) at 37°C for 15 min. The dissociated cells were seeded into 300 cm^2 plastic flasks at a density of 10^7 per 300 cm^2 in MEM or DMEM with 0.17% $NaHCO_3$ and 10% FCS and maintained at 37°C in 10% CO_2/90% air with a change of medium twice per week. After 10–14 days, floating cells and weakly attached cells on the mixed primary culture cell layer were obtained by gently shaking for 10–15 min. The resulting cell suspension was seeded onto glass coverslips and allowed to adhere for 30 min at 37°C. Then, microglia were isolated as strongly adhering cells after unattached cells were removed. The purity of microglia ranged from 95% to 99% according to the type of experiments. Special care was taken for PCR so that other cell types, for example, astrocytes and oligodendrocyte type 2 astrocyte (O-2A) progenitor cells, were not contaminated.

Cell Identification

Microglial cells were identified by a fluorescent probe, isolectin-B_4. Primary cultured microglia plated on the chamber slides were fixed with 4% paraformaldehyde for 30 min at room temperature, followed by a wash with phosphate-buffered saline (PBS). For the identification of microglia, the cells were treated with 10 μg/ml isolectin-B_4 overnight at 4°C, followed by 5 × wash with PBS. Then the cells were examined with a digital camera system (Axio Cam, Carl Zeiss, Germany) with high resolution mounted on a light and fluorescent microscope (Axioscope2 plus, Carl Zeiss).

Electrophysiological Measurements

Whole-cell recordings were made as reported previously (Noda et al., 1999, 2000) using an Axopatch-200B amplifier (Axon Instruments, Foster City, CA) under the voltage-clamp condition at the holding potential of −60 mV. The membrane currents were measured using a patch pipette containing (in mM): CsCl, 100; Na_2ATP, 3; N-2-hydroxyethylpiperazine-N′-2-ethan-

TABLE 1. Primer Pairs

Name (rat)	Accession number	Primer sequence	Between residues
GluR1/flip	M38060	GAAGCAAGGACTCCGGAAGTAA	2363 and 2384
		GTAGAACACGCCTGCCACATT	2433 and 2413
GluR1/flop	M36418	GTCCGCCCTGAGAAATCCA	2259 and 2277
		AGCCCCTGCTCGTTCAGTT	2315 and 2297
GluR2/flip	M38061	GGAACCCCAGTAAATCTTGCAGT	2720 and 2742
		GAGTCCTTGGCTCCACATTCAC	2826 and 2805
GluR2/flop	M36419	CATCGCCACACCTAAAGGATC	2262 and 2282
		CAATTTGTCCAACAGGCCTTGT	2349 and 2328
GluR3/flip	M38062	GGAATGTGGAGCCAAGGACTC	2391 and 2411
		GCTCAGGCTTAGAGCACTGGTC	2448 and 2427
GluR3/flop	M36420	GGCAACCCCTAAAGGCTCAG	2280 and 2299
		AATACTGCCAGGTTAACAGCATTTC	2330 and 2306
GluR4/flip	M38063	TTTTGAAACTCAGTGAGGCAGG	2315 and 2336
		CGTACCACCATTTGTTTTTCAGC	2371 and 2349
GluR4/flop	M36421	CCTCTTGGACAAATTGAAAAACAA	2337 and 2360
		CCGCTGCCACATTCTCCTT	2393 and 2375

sulphonic acid (HEPES), 5; $CaCl_2$, 1; $MgCl_2$, 4; ethyleneglycol-bis-N,N,N′,N′-tetraacetic acid (EGTA), 5; and N-methyl-D-glucamine (NMDG), 10. The pH of the solution was adjusted to 7.3 with 1 N HCl. The pipette resistance was 5–9 MΩ. The external solution contained (in mM): KCl, 2.5; NaCl, 110; $CaCl_2$, 3; $BaCl_2$, 6; glucose, 15; and HEPES, 5. The pH was adjusted to 7.4 with NMDG. The external KA or drugs were applied rapidly using the Y-tube technique (Min et al., 1996), which allows the complete exchange of the external solution surrounding a cell within 20 ms. The temperature monitored in the recording dishes was 33–34°C. PEPA and cyclothiazide were dissolved in DMSO at 0.1 or 0.3 M, and the solutions were diluted into the control medium to prepare working solutions. The maximal concentration of DMSO in the medium was 0.1%. The electrophysiological data are presented as mean ± SEM in the text and the SEM is indicated by a vertical bar in the figures.

SYBR Green-Based Real-Time Quantitative RT-PCR

Total RNAs were prepared from 2×10^6 microglial cells with RNeasy RNA purification kit (Qiagen, Valencia, CA) according to the manufacturer's protocol. First-strand cDNA synthesized from 1 μg total RNA with random hexamer primers was used as template for each reaction. SYBR Green-based real-time quantitative RT-PCR was performed as described (Aoki et al., 2002). Applied Biosystems 7700 Sequence Detection System (Foster City, CA) was used for the signal detection and the PCR was performed in 1 × SYBR Green Master mix with 500 nM of each primer (Applied Biosystems). For standardization and quantification, rat β-actin or GAPDH was amplified simultaneously. Primer sequences were designed with Primer Express Software (Applied Biosystems). The primer pairs for each GluRs-flip/flop were shown in Table 1.

PCR conditions were 95°C for 10 min, followed by 40 cycles at 95°C for 15 sec and 60°C for 1 min. The threshold cycle of each gene was determined as the PCR cycle at which an increase in fluorescence was observed above the baseline signal in an amplification plot (Wada et al., 2000). The normalized expression level of target (dCt) was calculated as the difference in threshold cycles for target and reference (β-actin or GAPDH). The formula 2^{-dCt} was used to calculate relative expression levels for target molecules compared to the reference. To reduce possible error, RT-PCR reaction was performed three times and averaged 2^{-dCt} values were obtained.

Assay of TNF-α

The isolated microglial cells were seeded in a 96-well plate at a density of 1.5×10^5 cells/ml and stabilized for 30 min. Then the cells were treated with 1 mM Glu or 300 μM KA with or without PEPA, CTZ, or PD 098059, an MAPK inhibitor. To see the effect of Ca^{2+}-free or Na^+-free solution, the following solutions were used (in mM); KCl, 2.5; NaCl, 110; $BaCl_2$, 6; glucose, 15; and HEPES, 5 (Ca^{2+}-free solution); and KCl, 2.5; choline Cl, 110; $CaCl_2$, 3; $BaCl_2$, 6; glucose, 15; and HEPES, 5 (Na^+-free solution). The pH of the solution was adjusted to 7.4 with NMDG. After treatment for 3 h, the amount of rat TNF-α released into the culture medium was measured using an ELISA Kit following the manufacturer's protocol (Biosource, Camarillo, CA). The absorbency at 450 nm was measured with a Microplate Reader (ImmunoMini NJ-2300, Narge Nunc International, Denmark). The data are presented as mean ± SEM of 4–5 experiments.

Immunocytochemistry

Microglial cells cultured on glass coverslips were initially rinsed three times for 5 min per rinse with PBS. Cells were fixed with freshly prepared 4% paraformaldehyde for 30 min at room temperature. Following several rinses with PBS, the cells were permeated with 0.1% Triton-X-100 in PBS for 15 min, then incubated for 60 min in a blocking solution containing 2% bovine

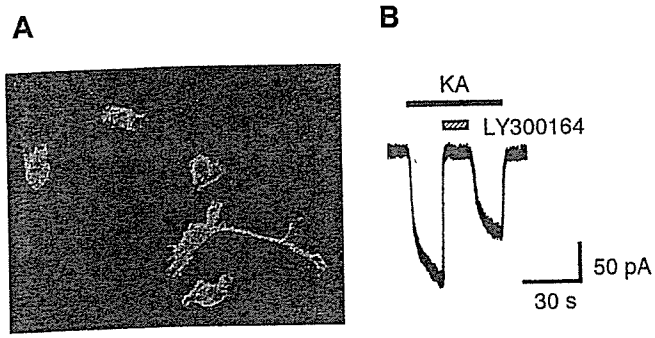

Fig. 1. Identification of microglia and KA-induced current. **A:** Microglial cells were identified using fluorescent probe isolectin-B_4 under the fluorescent microscope combined with phase-contrast modes. Scale bar = 12.5 μm. **B:** Membrane current induced by 300 μM KA was completely blocked by 100 μM LY300164, a selective antagonist of AMPA receptors. The holding potential was −60 mV. Similar results were obtained in four other cells.

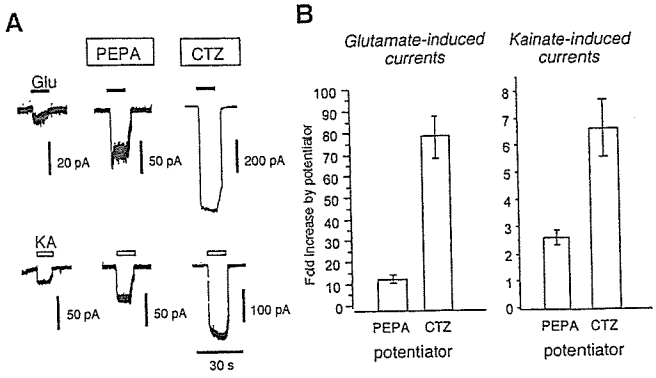

Fig. 2. Potentiating effect of PEPA and CTZ on AMPA receptor in microglial cells. **A:** Effect of PEPA (100 μM) and CTZ (100 μM) on Glu (300 μM)- and KA (300 μM)-induced inward current. The holding potential was −60 mV. All currents were induced in one cell. Similar results were obtained in three other cells. Note the different calibrations. **B:** Effect of each potentiator (100 μM) on Glu (300 μM)- and KA (300 μM)-induced currents recorded at −60 mV. Each bar represents mean ± SEM.

serum albumin (BSA) plus 2% FCS in PBS. Following 3 × rinses with 1% BSA in PBS, the cells were incubated overnight at 4°C with primary antibody diluted in 1% BSA in PBS. The primary antibodies used was rabbit anti–rat TNF-α (1:100; Endogen, MA). Subsequently, cells were rinsed six times for 5 min per rinse, with 1% BSA in PBS and then incubated with Alexa Fluor 594-coupled secondary antibodies (1:500; Molecular Probes, Eugene, OR) for 60 min. Following further wash of six times with 1% BSA in PBS and a final wash with PBS alone, the coverslips were mounted on ethanol-cleaned slides using fluorescence mounting medium (Vector Laboratories, CA) and visualized using a fluorescent microscope system as mentioned above. Images were obtained using a 40× objective with the acquisition setting at 1,300 × 1,030 pixels resolution. Control experiments in which the primary antibody was omitted were performed to determine antibody specificity.

RESULTS

AMPA-Type Glutamate Receptors in Microglia

Most of the isolated cells were microglia (~ 99%) and showed small round- or rod-shaped cell bodies with no or a few thick processes (Fig. 1A). We observed Glu- or KA-induced currents in whole-cell patched microglial cells under voltage-clamp conditions at the holding potential of −60 mV. KA induces a nondesensitizing inward current through AMPA receptors (Patneau and Mayer, 1990). In the previous study, KA induced sustained inward currents in a concentration-dependent manner with half-activation concentration of 330 μM, and the response to 300 μM KA was totally suppressed in the presence of 10 μM CNQX (Noda et al., 2000). In the previous study, it was predicted that KA-induced currents were mainly due to AMPA receptors because of low responsiveness to concanavalin A. In the present study, KA-induced currents were completely blocked by LY300164 (100 μM), a selective antagonist of AMPA receptors (Czuczwar et al., 1998), suggesting that most of the functional glutamate receptors in cultured rat microglia were revealed to be AMPA receptors, but not KA receptors (n = 5; Fig. 1B).

Effect of PEPA and Cyclothiazide on Glutamate- and Kainate-Induced Currents in Microglia

We studied the effect of PEPA and CTZ on Glu- and KA-induced currents in whole-cell patched microglial cells (Fig. 2A). It has been shown that both modulators produced marked potentiation of AMPA-preferring receptor-mediated response (Sekiguchi et al., 1997, 1998; Shen et al., 1999). Each of glutamate receptor agonists (Glu or KA, 300 μM) was first applied to microglial cell, and after 3-min wash, PEPA (100 μM) or CTZ (100 μM) was preloaded for 1 min. Then, each agonist was again applied in the presence of PEPA or CTZ (each solution was applied after 3-min wash). Since we could not observe the fast transient peak of AMPA receptor current, we measured the amplitudes of steady-state component of the Glu responses. Therefore, the potentiating ratios of Glu-induced currents were overestimated compared to those of KA-induced currents. Both PEPA and CTZ clearly potentiated the steady-state level of Glu- and KA-induced currents. However, PEPA was much less potent than CTZ in rat microglia.

The potentiating effects of PEPA and CTZ were summarized in Figure 2B. Figure 2B (left) shows the effect of the modulators on Glu-induced sustained currents. The potentiation by PEPA and CTZ was 15.2 ± 2.0 fold (n = 30) and 79.2 ± 9.7 fold (n = 17), respectively. Similarly, Figure 2B (right) shows the effect on KA-induced currents. The extent of potentiation of KA-induced currents by both modulators was much weaker

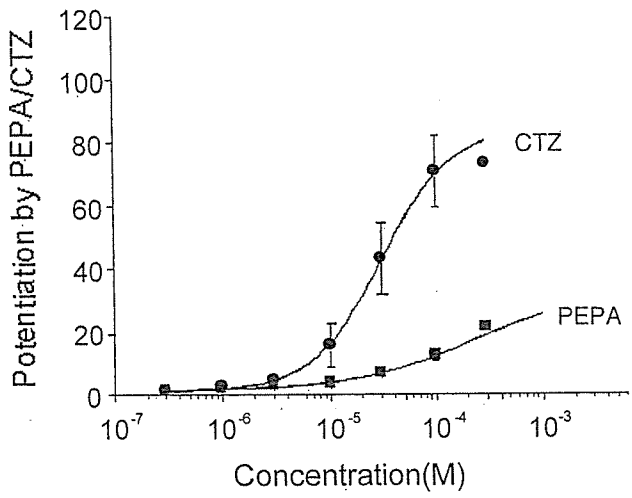

Fig. 3. Dose-dependent potentiation of Glu-induced currents by PEPA and CTZ. The potentiation by PEPA (squares) or by CTZ (circles) was calculated as follows: current amplitude induced by Glu (300 μM) plus PEPA or CTZ/current amplitude induced by Glu (300 μM) alone. The theoretical curves indicate the best fit to the data according to logistic function, $I = I_{max} \times 1/[1 + (EC_{50}/ligand)^n]$. Values are mean ± SEM (n = 4–20).

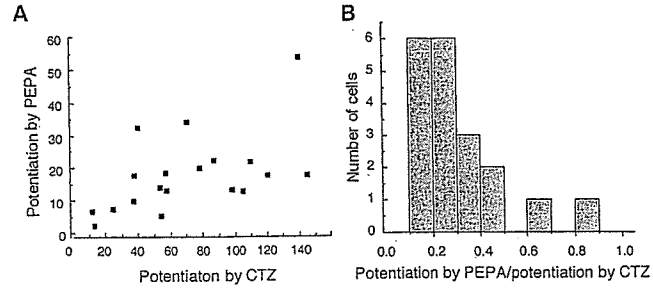

Fig. 4. Distribution of P/C ratio. **A:** A scatter plot illustrating potentiation by PEPA of Glu-induced inward current versus potentiation by CTZ of Glu-induced inward current in each of the cultured microglial cells tested (n = 19). **B:** The distribution of P/C ratio among the rat cultured microglia. Abscissa scale shows P/C ratio, which was calculated as follows: potentiation by 100 μM PEPA (as calculated above)/potentiation by 100 μM CTZ (as calculated above). Ordinate scale shows number of cells.

than that of Glu-evoked currents: PEPA 2.7 ± 0.3 fold (n = 11) and CTZ 6.7 ± 1.1 fold (n = 8).

Concentration-Dependent Potentiation of Glu-Induced Currents by PEPA and CTZ

PEPA potentiated Glu-induced currents in a dose-dependent manner (Sekiguchi et al., 1997; Shen et al., 1999). Figure 3 shows the fold increase of Glu (300 μM)-induced currents by PEPA and CTZ with different concentration. Both PEPA (10^{-6} to 10^{-3} M) and CTZ (10^{-6} to 10^{-3} M) potentiated Glu-induced currents in a concentration-dependent manner in rat microglial cells. The EC_{50} for potentiation by PEPA and CTZ were 210 μM (Hill coefficient = 0.79) and 31 μM (Hill coefficient = 1.32), respectively.

Heterogeneity of AMPA Receptor in Microglia

It has been reported that a comparison of the action of PEPA versus CTZ (P/C ratio) facilitates the detection of the splice variant heterogeneity of AMPA receptors in rat hippocampal cultures (Sekiguchi et al., 1998). Xenopus oocytes expressing recombinant AMPA receptors predominantly composed of flip splice variants showed lower P/C ratios (0.19–0.50), while those consisting of flop variants showed higher P/C ratios (1.8–2.2) (Sekiguchi et al., 1998). According to the previous report, we investigated the cell-to-cell variations of flip and flop variants of AMPA receptors in rat microglia. The scatter plots in Figure 4A illustrated the potentiation by PEPA versus potentiation by CTZ of Glu-induced currents in each of the cultured microglial cells (n = 19). The potentiation by PEPA and potentiation by CTZ showed pronounced cell-to-cell variations. The population of Glu-induced currents by PEPA varied between 2.5- and 54-fold, and the potentiation by CTZ varied between 11.3- and 145-fold (Fig. 4A). The histogram in Figure 4B, which was plotted from the data shown in Figure 4A, shows the number of cells included in each range of the P/C ratio. The cultured microglia we used showed cell-to-cell variations with respect to the P/C ratio (0.1–0.9). In contrast to the results in hippocampal neurons (Sekiguchi et al., 1998), most of microglial cells (17/19 cells, 89%) exhibited P/C ratios of lower than 0.5. These results suggest that the heterogeneity of microglial cells may be more restricted than that of hippocampal neurons.

Expression of AMPA Receptor Subunits and Their Splice Variants in Rat Microglia

To prepare the microglial cell culture for RT-PCR study, great care was taken to eliminate the contamination of other cell types so that the purity was more than 99%. Quantitative RT-PCR analysis of AMPA receptors showed that rat primary cultured microglia express substantial amount of flip variants of GluR1–4 and flop variant of GluR2 and GluR4 (Fig. 5). In contrast, flop variant of GluR1 and GluR3 were barely detected. Overall, flip variants of GluRs appear to be expressed dominantly in rat cultured microglia, in accordance with the results that CTZ was a more potent enhancer of AMPA receptors in rat microglia.

Current-Voltage Relationship of Glu-Induced Currents and Effect of PEPA and CTZ

Figure 6 shows the current-voltage (I-V) relationship of the Glu (300 μM)-induced response in the absence or presence of the modulators (100 μM). The microglial cells were voltage-clamped at −60 mV. The I-V rela-

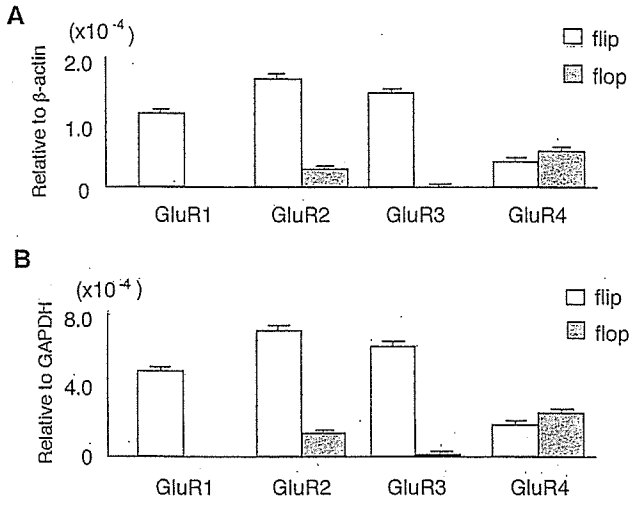

Fig. 5. Quantitative RT-PCR of GluR1–4 and their splice variances (flip/flop). The expression level of each receptor mRNA was normalized to the level of β-actin mRNA (**A**) or GAPDH mRNA (**B**) and was shown as relative values when β-actin or GAPDH mRNA level is 1.

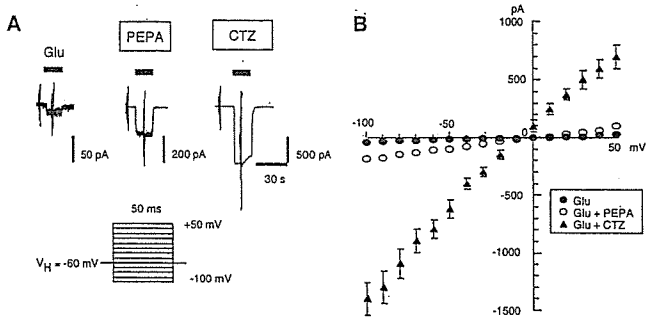

Fig. 6. I-V relationship of Glu-induced currents. **A:** 300 μM Glu-induced currents in the absence and presence of 100 μM PEPA or CTZ were obtained and voltage pulses with 50-ms duration were applied between −100 and 50 mV from the holding potential of −60 mV (shown below) before and during the application of Glu. **B:** The voltage-dependence of Glu-induced currents was obtained by subtracting the currents before application of Glu. Each point represents the mean ± SEM (n = 3).

tionships were obtained at membrane potentials between 50 mV and −100 mV in 10 mV steps with 50-ms duration before and during application of Glu in the absence or presence of modulators. The current amplitude was measured at the end of each pulse (Fig. 6A). Glu-induced I-V was obtained by subtracting the current before application of Glu, which reversed approximately at 0 mV under each condition (Fig. 6B). PEPA and CTZ potentiated the amplitude of AMPA receptor responses with little change in ionic permeability.

Inhibition of Glu- and KA-Activated Release of TNF-α From Microglia by PEPA and CTZ

Microglial cells are known to produce cytokines after cellular activation (McGeer et al., 1993; Meda et al., 1995). When microglial cells were activated with Glu or KA, the production of TNF-α was significantly enhanced (Noda et al., 2000). Accordingly, we predicted that the production of TNF-α would significantly increase when the Glu- or KA-induced currents were significantly enhanced. However, we found that this was not the case in our study. Surprisingly, the production of TNF-α by Glu or KA was rather suppressed in the presence of PEPA or CTZ (Fig. 7A). Similar to our previous report, the production of TNF-α was significantly enhanced by 1 mM Glu or KA after 3-h incubation. However, when PEPA or CTZ at the concentration of 100 μM were added, the production of TNF-α was suppressed, especially with CTZ. The production of TNF-α in the presence of PEPA or CTZ alone was the same as the control (data not shown). Immunostaining of TNF-α using anti-TNF-α-specific antibody showed strong induction of TNF-α by application of 1 μg/ml lipopolysaccharide, which also triggers microglial chemokine and cytokine. The moderate increase in TNF-α was observed by 1 mM Glu. In accordance with the result in Figure 7A, application of Glu together with 100 μM CTZ nullified the induction of TNF-α (Fig. 7B).

To investigate the contribution of excess influx of Na^+ or Ca^{2+} ions to the inhibition of TNF-α release by CTZ, the culture medium was exchanged by Na^+-free or Ca^{2+}-free solution and TNF-α assay was performed the same way. The increase in TNF-α release by Glu or KA was not observed when extracellular Na^+ or Ca^{2+} ions were eliminated (Fig. 8A). Coapplication of CTZ at concentration of 10 or 100 μM did not have significant effect either. In both Na^+-free and Ca^{2+}-free solution, the absolute amounts of control TNF-α release were much higher than those obtained in the culture medium. The reason was not known but it was predicted that Na^+-free or Ca^{2+}-free conditions might be stressful circumstances for microglia and hence microglia was activated to release TNF-α. Even under these circumstances, application of microglial cells with 100 ng/ml LPS caused 5–6 times increase in TNF-α release (data not shown). These results suggest that influx of Na^+ and Ca^{2+}-ions through AMPA receptor is important for Glu-induced increase in TNF-α release.

TNF-α release by Glu or KA may be due to MAPK activation as was reported by corticotropin releasing hormone (Wang et al., 2003). In this case, the inhibitory effects of PEPA and CTZ might be due to the inhibition of MAPK. However, TNF-α release by Glu (not shown) or KA was not affected by preapplication of microglia with 5 μM PD 098059, an MAPK inhibitor, for 24 h (Fig. 8B). Our result suggests that activation of MAPK was not required for the Glu-induced TNF-α release and therefore MAPK inhibitor did not mimic the inhibitory effects of CTZ or PEPA.

DISCUSSION

Although properties of cultured microglia can considerably differ from corresponding cells in situ, the present study confirmed that rat microglia express

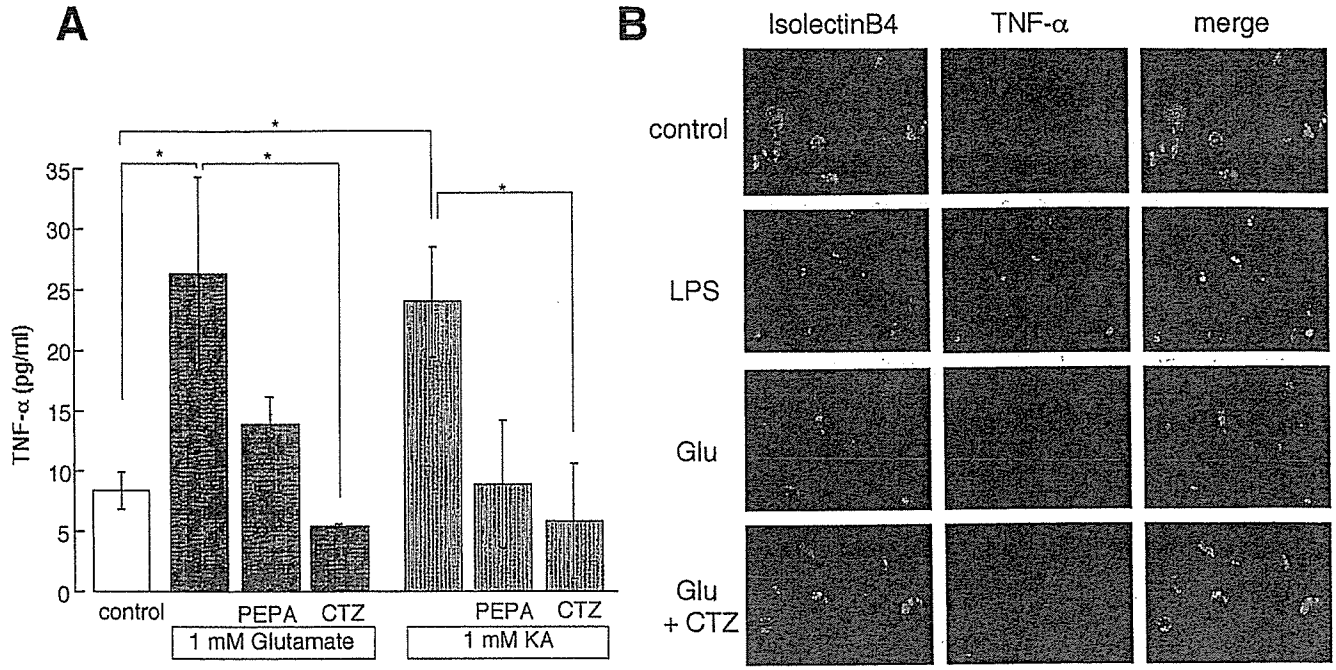

Fig. 7. Effects of PEPA and CTZ on Glu- and KA-induced TNF-α release. **A:** The amount of TNF-α released into the culture medium was measured by ELISA. Production of TNF-α by 1 mM Glu or KA was rather attenuated by addition of PEPA (100 μM) or CTZ (100 μM). Asterisk, $P < 0.05$ compared with control (one-way ANOVA). **B:** Immunofluorescence of TNF-α in microglia treated with 1 μg/ml LPS, 1 mM Glu, or 100 μM CTZ together with 1 mM Glu for 3 h. Microglial cells were double-stained with isolectin-B_4 (FITC-labeled: green) and anti-TNF-α antibody (Alexa Fluor 594-labeled; red).

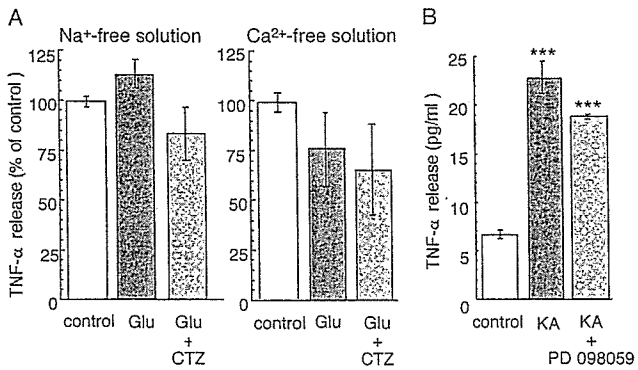

Fig. 8. Effects of Na^+- and Ca^{2+}-free extracellular solution and MAPK inhibitor on TNF-α release. **A:** TNF-α release was not significantly activated by Glu in Na^+-free solution and even cancelled in Ca^{2+}-free solution. Coapplication of CTZ tended to attenuate the TNF-α release further. **B:** Preapplication of microglial cells with an MAPK inhibitor, PD 098059 (5 μM), did not have significant effect on KA-activated TNF-α release. Triple asterisk, $P < 0.001$ compared with control (one-way ANOVA).

AMPA-type Glu receptors and found that little functional KA receptors were expressed by using a new AMPA-selective inhibitor. In a previous report (Noda et al., 2000), RT-PCR study suggested that rat microglia might also express KA-type Glu receptors. Using KA as an agonist of AMPA/KA type of Glu receptor, which gave noninactivating inward currents, we introduced the specific inhibitor of AMPA-type Glu receptors, LY300164, which corresponds to GYKI53773 and a noncompetitive antagonist of AMPA receptor-mediated responses (Czuczwar et al., 1998; Abraham et al., 2000). In our study, the sustained inward current in the presence of 300 μM KA was completely inhibited by 100 μM LY300164 in five cells tested (Fig. 1), as shown in cultured rat spinal cord motoneurons (Van Damme et al., 2002). These results confirmed that KA-induced currents in cultured rat microglia were mostly AMPA receptor-mediated currents and KA receptors were barely functional, though concanavalin-sensitive KA receptors could be recorded in some cells (Noda et al., 2000).

The AMPA receptor-mediated responses either by Glu or KA were greatly enhanced by PEPA and CTZ (Fig. 2), and the effects of PEPA and CTZ were concentration-dependent (Fig. 3). Figure 2B compares the action of PEPA and CTZ on Glu- and KA-evoked currents. Glu responses were smaller than KA responses in the absence of modulators (Fig. 2A; left traces). This is attributable in part to stronger desensitization of responses to glutamate than KA at AMPA receptors (Patneau and Mayer, 1991; Patneau et al., 1993). Since we could not observe fast transient currents with our Y-tube system, all respective quantification was done at the steady-state components, which usually reach less than 10% of the effective amplitudes. Consequently, the overall amplification by PEPA and CTZ appear to be overestimated. Though there was a limitation of measurement system, smaller potentiation by PEPA on both Glu- and KA-induced currents than that by CTZ was observed.

Our results revealed that microglial cells consist of multiple populations with respect to P/C ratio (Fig. 4), which suggests that multiple AMPA receptor subtypes are expressed in the cultured microglia we used. The P/C ratio varies with subunit and splice variant compositions. Our investigation in microglia gave relatively low P/C ratio (0.1–0.9) with most abundant distribution between 0.1 and 0.5 (89%). The low P/C ratio results from a combination of the weak potentiation by PEPA and potent action by CTZ. Since CTZ and PEPA act preferentially on flip and flop variants, respectively, cells exhibiting a low P/C ratio (< 0.5) are supposed to express flip variants predominantly. In the cultured hippocampal cells, two populations exhibited characteristic P/C ratio: low P/C ratio (0–0.15, 34%) and high P/C ratio (> 2.00, 1%) with intermediate P/C ratio (0.25–1.20, 65%) (Sekiguchi et al., 1998). Taken together, the distribution of different combination of flip/flop variants were more restricted in microglia than hippocampal cells.

Our electrophysiological observation that rat microglia may express flip variants preferentially was further confirmed by quantitative RT-PCR (Fig. 5). The P/C ratio of 0.1–0.5 in the majority of the cultured microglia is likely explained by the predominant expression of flip forms as shown in oocytes expressing GluR1-3 (Sekiguchi et al., 1998). In addition, GluR4 variants may contribute to not only heterogeneity but also activation of microglia (Mennini et al., 2002).

We previously reported that rat microglia express GluR2 and showed low Ca^{2+} permeability with or without CTZ (Noda et al., 2000). It is well known that AMPA receptor lacking GluR2 (RNA-edited form) conduct calcium ions (Hollmann et al., 1991; Hume et al., 1991; Burnashev et al., 1992). In the present study, we applied series of short pulses to obtain quick I-V relationships instead of changing the holding potential. The I-V relationships of Glu-induced currents in rat microglia were quite similar to those we obtained before and were quite linear in the presence of PEPA as well. It confirms that both PEPA and CTZ do not affect rectification or ion permeability of AMPA receptors (Fig. 6).

Activation of microglia is often observed in pathological conditions. Regulation of microglial reactivity has been proposed to be a key factor for neuroprotection in brain disorders, including neurodegenerative diseases (Streit and Kincaid-Colton, 1995; Wyss-Coray et al., 2001; Polazzi and Contestabile, 2002). Though the physiological role of AMPA receptor in microglia still remains unclear, the enhancement of AMPA receptor in microglia may have a possibility to contribute to neuroprotection. Actually, PEPA ameliorates postischemic memory impairment even with ischemia-induced structural damage to the brain (Sekiguchi et al., 2001). In the present study, we unexpectedly observed that coapplication of PEPA with Glu attenuated the TNF-α release stimulated by Glu or KA alone in microglia. More surprisingly, coapplication of CTZ with Glu or KA almost completely nullified the increase in TNF-α release (Fig. 7A). It means that augmentation of AMPA-induced currents has negative feedback control on the release of TNF-α, though the mechanism is not known yet. The inhibition rate of TNF-α release was not significantly different between 10 and 100 μM of PEPA or CTZ (not shown), suggesting the concentration dependence of PEPA and CTZ on TNF-α release might be different from that on current augmentation.

The mechanism of Glu- or KA-activated TNF-α release was still unknown. However, the new aspects that extracellular Na^+ and Ca^{2+} ions are required for Glu- or KA-induced TNF-α release were obtained (Fig. 8A). It was reported that Na^+ entry through AMPA receptors results in voltage-gated K^+ channel blockade in glial cells (Borges and Kettenmann, 1995; Schröder et al., 2002). Since voltage-dependent K^+ currents in microglia were small in our experimental condition and it was reported that resting microglia did not have outward K^+ currents (Kettenmann et al., 1993), it was hard to distinguish whether potentiation of AMPA receptor caused the inhibition of voltage-dependent K^+ channel or not. Apart from the effects on K^+ channels, it may be predicted that excess influx of Na^+ ions could cause inhibitory effects on subsequent function in microglia with unknown mechanism. Indeed. elimination of Na^+ not only prevented the effects of PEPA and CTZ but also Glu- or KA-activated TNF-α release itself. Elimination of extracellular Ca^{2+} ions had more clear effect on the inhibition of Glu-activated TNF-α release, as was predicted by the report that intracellular Ca^{2+} ions were important in TNF-α production (Fig. 8A, right) (Combs et al., 1999). We further investigated whether PEPA or CTZ had inhibitory effects on TNF-α release by other stimulant, for example, lipopolysaccharide (LPS). However, there was no significant inhibition by PEPA or CTZ, even in the presence of Glu (data not shown). Therefore, the inhibitory effect of PEPA and CTZ was not a nonspecific effect on general production of TNF-α, and the inhibitory effect due to the augmentation of AMPA receptor could not compete with LPS-activated TNF-α.

Another question was whether Glu-activated TNF-α release was MAPK-dependent or not. Because it was reported that LPS-induced TNF-α release was augmented by p38 MAPK (Lee et al., 2000), the effect of PEPA or CTZ could be due to the modulation of MAPK activity. However, application of one of the MAPK-inhibitor, PD 098059, to microglial cells did not significantly affect Glu-activated TNF-α release. Immunoreactivity of phospho-p38 MAPK also showed no difference between the control, Glu-treated, and Glu with CTZ-treated rat cultured microglia (data not shown). These results indicate that the Glu-induced TNF-α release and their modulation by CTZ were independent on MAPK activity.

The contribution of metabotropic Glu receptors (mGluRs) to the formation of TNF-α could also be plausible. Though Glu- and KA-induced TNF-α release was significantly inhibited by CNQX (Noda et al., 2000), expression of mGluRs in microglia was already re-

ported (Biber et al., 1999; Taylor et al., 2002, 2003; Venero et al., 2002). In addition, reduction of TNF-α as well as K^+ currents and NO synthesis was shown in microglia after activation of purinergic receptors (Boucsein et al., 2003).

It is interesting that microglia survived in the presence of CTZ even after 3-h incubation together with Glu (not shown). Low Ca^{2+} permeability of the AMPA receptors may contribute to the survival of microglia. CTZ was reported to cause neuronal and astrocytic cell death due to an excess Ca^{2+} influx into the cells (Brorson et al., 1995; David et al., 1996; John et al., 1999). In contrast to CTZ, PEPA was reported to ameliorate postischemic memory impairment in rats (Sekiguchi et al., 2001). The ameliorating effect of PEPA may not simply be explained by milder blocking of the desensitization of AMPA receptors in neurons. Therefore, we expected that analyzing the effects of PEPA and CTZ on AMPA receptors in microglia might help us understand the effect of these modulators. In addition to the effect on TNF-α, it will be worth trying to investigate how PEPA and CTZ affect the release of other cytokines and growth factors from microglia.

As a conclusion, allosteric modulators of flip and flop type of AMPA receptors are useful tools for detecting the heterogeneity of microglia. Besides, these modulators had inhibitory effect on Glu- or KA-activated TNF-α, though the mechanism was not yet known. Since microglia amplify the release of TNF-α from astrocyte, which was shown in cocultures of astocyte-microglia (Bezzi et al., 2001), and has important role in neuron-glial communication (Fields and Stevens-Graham, 2002), further studies on the effects of modulators in glia-glia or neuron-glia interaction will help us understand the functional role of AMPA receptors in microglia and the difference between CTZ and PEPA in their ameliorating effect in ischemic brain.

ACKNOWLEDGMENTS

The authors thank Dr. T. Harada for his help in their initial experiments, Dr. H. Nakanishi (Kyushu University) for valuable suggestions on the preparation of the primary cultured microglia, Professor N. Akaike (Kyushu University) for providing some of the equipments, and Professor D.A. Brown (University College, London) for reading the manuscript.

REFERENCES

Abraham G, Solyom S, Csuzdi E, Berzsenyi P, Ling I, Tarnawa I, Hamori T, Pallagi I, Horvath K, Andrasi F, Kapus G, Harsing LG Jr, Kiraly I, Patthy M, Horvath G. 2000. New non competitive AMPA antagonists. Bioorg Med Chem 8:2127–2143.

Aoki K, Sun YJ, Aoki S, Wada K, Wada E. 2002. Cloning, expression, and mapping of a gene that is upregulated in adipose tissue of mice deficient in bombesin receptor subtype-3. Biochem Biophys Res Commun 290:1282–1288.

Bezzi P, Domercq M, Brambilla L, Galli R, Schols D, De Clercq E, Vescovi A, Bagetta G, Kollias G, Meldolesi J, Volterra A. 2001. CXCR4-activated astrocyte glutamate release via TNF-alpha: amplification by microglia triggers neurotoxicity. Nat Neurosci 4:702–710.

Biber K, Laurie DJ, Berthele A, Sommer B, Tolle TR, Gebicke-Harter PJ, van Calker D, Boddeke HW. 1999. Expression and signaling of group I metabotropic glutamate receptors in astrocytes and microglia. J Neurochem 72:1671–1680.

Borges K, Kettenmann H. 1995. Blockade of K^+ channels induced by AMPA/kainate receptor activation in mouse oligodendrocyte precursor cells is mediated by Na^+ entry. J Neurosci Res 42:579–593.

Boucsein C, Zacharias R, Farber K, Pavlovic S, Hanisch UK, Kettenmann H. 2003. Purinergic receptors on microglial cells: functional expression in acute brain slices and modulation of microglial activation in vitro. Eur J Neurosci 17:2267–2276.

Brorson JR, Manzolillo PA, Gibbons SJ, Miller RJ. 1995. AMPA receptor desensitization predicts the selective vulnerability of cerebellar Purkinje cells to excitotoxicity. J Neurosci 15:4515–4524.

Burnashev N, Monyer PH, Seeburg B, Sackmann B. 1992. Diavalent ion permeability of AMPA receptor channels is dominated by edited of a single subunit. Neuron 8:189–198.

Combs CK, Johnson DE, Cannady SB, Lehman TM, Landreth GE. 1999. Identification of microglial signal transduction pathways mediating a neurotoxic response to amyloidogenic fragments of β-amyloid and prion proteins. J Neusosci 19:928–939.

Czuczwar SJ, Swiader M, Kuzniar H, Kleinrok Z. 1998. LY300164, a novel antagonist of AMPA/kainite receptors, potentiates the anticonvulsive activity of antiepileptic drugs. Eur J Pharmacol 359: 103–109.

David JC, Yamada KA, Bagwe MR, Goldberg MP. 1996. AMPA receptor activation is rapidly toxic to cortical astrocytes when desensitization is blocked. J Neurosci 16:200–209.

Fields RD, Stevens-Graham B. 2002. New insights into neuron-glia communication. Science 298:556–562.

Hollmann M, O'Shea-Greenfield A, Rogers SW, Heinemann S. 1989. Cloning by functional expression of a member of the glutamate receptor family. Nature 342:643–648.

Hollmann M, Hartley S, Heinemann S. 1991. Ca^{2+} permeability of KA-AMPA-gated glutamate receptor channels depends on subunit composition. Science 252:851–853.

Hume RI, Dingledine R, Heinemann SF. 1991. Identification of a site in glutamate receptor subunits that controls calcium permeability. Science 253:1028–1031.

John CA, Beart PM, Giardina SF, Pascoe CJ, Cheung NS. 1999. Cyclothiazide and GYKI 52466 modulate AMPA receptor-mediated apoptosis in cortical neuronal cultures. Neurosci Lett 268:9–12.

Keinanen K, Wisden W, Sommer B, Werner P, Herb A, Verdoorn TA, Sakmann B, Seeburg PH. 1990. A family of AMPA-selective glutamate receptors. Science 249:556–560.

Kessler M, Rogers G, Arai A. 2000. The norbornenyl moiety of cyclothiazide determines the preference for flip-flop variants of AMPA receptor subunits. Neurosci Lett 287:161–165.

Kettenmann H, Banati R, Walz W. 1993. Electrophysiological behavior of microglia. Glia 7:93–101.

Kreutzberg GW. 1996. Microglia: a sensor for pathological events in the CNS. Trends Neurosci 19:312–318.

Lee YB, Schrader JW, Kim SU. 2000. p38 map kinase regulates TNF-alpha production in human astrocytes and microglia by multiple mechanisms. Cytokine 12:874–880.

McGeer PL, Kawamata T, Walker DG, Akiyama H, Tooyama I, McGeer EG. 1993. Microglia in degenerative neurological disease. Glia 7:84–92.

Meda L, Cassatella MA, Szendrei GI, Otvos L Jr, Baron P, Villalba M, Ferrari D, Rossi F. 1995. Activation of microglial cells by beta-amyloid protein and interferon-gamma. Nature 374:647–650.

Mennini T, Bigini P, Ravizza T, Vezzani A, Calvaresi N, Tortarolo M, Bendotti C. 2002. Expression of glutamate receptor subtypes in the spinal cord of control and mnd mice, a model of motor neuron disorder. J Neurosci Res 70:553–560.

Min BI, Kim CJ, Rhee JS, Akaike N. 1996. Modulation of glycine-induced chloride current in acutely dissociated rat periaqueductal gray neurons by μ-opioid agonist DAGO. Brain Res 734:72–78.

Mosbacher J, Schoepfer R, Monyer H, Burnashev N, Seeburg PH, Ruppersberg JP. 1994. A molecular determinant for submillisecond desensitization in glutamate receptors. Science 266:1059–1062.

Noda M, Nakanishi H, Akaike N. 1999. Glutamate release from microglia via glutamate transporter is enhanced by amyloid-β peptide. Neuroscience 92:1465–1474.

Noda M, Nakanishi H, Nabekura J, Akaike N. 2000. AMPA-kainate subtypes of glutamate receptor in rat cerebral microglia. J Neurosci 20:251–258.

Partin KM, Patenau DK, Mayer ML. 1994. Cyclothiazide differentially modulates desensitization of AMPA receptor splice variants. Mol Pharmacol 46:129–138.

Partin KM, Fleck MW, Mayer ML. 1996. AMPA receptor flip/flop mutants affecting deactivation, desensitization, and modulation by cyclothiazide, aniracetam, and thiocyanate. J Neurosci 16:6634–6647.

Patneau DK, Mayer ML. 1990. Structure-activity relationships for amino acid transmitter candidates acting at N-methyl-D-aspartate and quisqualate receptors. J Neurosci 10:2385–2399.

Patneau DK, Mayer ML. 1991. Kinetic analysis of interactions between kainate and AMPA: evidence for activation of a single receptor in mouse hippocampal neurons. Neuron 6:785–798.

Patneau DK, Vyklicky L Jr, Mayer ML. 1993. Hippocampal neurons exibit cyclothiazide-sensitive rapidly desensitizing responses to kainite. J Neurosci 13:3496–3509.

Polazzi E, Contestabile A. 2002. Reciprocal interactions between microglia and neurons: from survival to neuropathology. Rev Neurosci 13:221–242.

Schröder W, Seifert G, Huttmann K, Hinterkeuser S, Steinhauser C. 2002. AMPA receptor-mediated modulation of inward rectifier K^+ channels in astrocytes of mouse hippocampus. Mol Cell Neurosci 19:447–458.

Sekiguchi M, Mark WF, Mark LM, Takeo J, Chiba Y, Yamashita S, Wada K. 1997. A novel allosteric potentiator of AMPA receptors: 4-[2-(phenylsulfonylamino)ethylthio]-2,6-difluoro-phenoxyacetamide. J Neurosci 17:5760–5771.

Sekiguchi M, Takeo J, Harada T, Morimoto T, Kudo Y, Yamashita S, Kohsaka S, Wada K. 1998. Pharmacological detection of AMPA receptor heterogeneity by use of two allosteric potentiators in rat hippocampal cultures. Br J Pharmacol 123:1294–1303.

Sekiguchi M, Yamada K, Jin J, Hachitanda M, Murata Y, Namura S, Kamichi S, Kimura I, Wada K. 2001. The AMPA receptor allosteric potentiator PEPA ameliorates post-ischemic memory impairment. Neuroreport 12:2947–2950.

Sekiguchi M, Nishikawa K, Aoki S, Wada K. 2002. A desensitization-selective potentiator of AMPA-type glutamate receptors. Br J Pharmacol 136:1033–1041.

Shen Y, Lu T, Yang X-L. 1999. Modulation of desensitization at glutamate receptors in isolated crucian carp horizontal cells by concanavalin A, cyclothiazide, aniracetam and PEPA. Neuroscience 89:979–990.

Sommer B, Keinanen K, Verdoorn TA, Wisden W, Burnashev N, Herb A, Kohler M, Takagi T, Sakmann B, Seeburg PH. 1990. Flip and flop: a cell-specific functional switch in glutamate operated channels of the CNS. Science 249:1580–1585.

Streit WJ, Kincaid-Colton CA. 1995. The brain's immune system. Sci Am 273:54–61.

Sun Y, Olson R, Horning M, Armstrong N, Mayer M, Gouaux E. 2002. Mechanism of glutamate receptor desensitization. Nature 417:245–253.

Taylor DL, Diemel LT, Cuzner ML, Pocock JM. 2002. Activation of group II metabotropic glutamate receptors underlies microglial reactivity and neurotoxicity following stimulation with chromogranin A, a peptide up-regulated in Alzheimer's disease. J Neurochem 82:1179–1191.

Taylor DL, Diemel LT, Pocock JM. 2003. Activation of microglial group III metabotropic glutamate receptors protects neurons against microglial neurotoxicity. J Neurosci 23:2150–2160.

Van Damme P, Van Den Bosch L, Van Houtte E, Eggermont J, Callewaert G, Robberecht W. 2002. Na(+) entry through AMPA receptors results in voltage-gated K(+) channel blockade in cultured rat spinal cord motoneurons. J Neurophysiol 88:965–972.

Venero JL, Santiago M, Tomas-Camardiel M, Matarredona ER, Cano J, Machado A. 2002. DCG-IV but not other group-II metabotropic receptor agonists induces microglial BDNF mRNA expression in the rat striatum. Correlation with neuronal injury. Neuroscience 113: 857–869.

Wada R, Tifft CJ, Proia RL. 2000. Microglial activation precedes acute neurodegeneration in Sandhoff disease and is suppressed by bone marrow transplantation. Proc Natl Acad Sci USA 97:10954–10959.

Wang W, Ji P, Dow KE. 2003. Corticotropin-releasing hormone induces proliferation and TNF-alpha release in cultured rat microglia via MAP kinase signalling pathways. J Neurochem 84:189–195.

Wyss-Coray T, Lin C, Yan F, Yu GQ, Rohde M, McConlogue L, Masliah E, Mucke L. 2001. TGF-beta1 promotes microglial amyloid-beta clearance and reduces plaque burden in transgenic mice. Nat Med 7:612–618.